國 立 交 通 大 學

電信工程學系

博 士 論 文

小型之寬頻一百八十度混合式耦合器及其
應用於寬頻耦合器與濾波器之設計

A Compact Wideband 180^0 Hybrid Coupler
and Its Applications to Wideband Coupler and
Bandpass Filter Designs

研究生：紀鈞翔 (Chun-Hsiang Chi)

指導教授：張志揚 (Chi-Yang Chang)

中 華 民 國 九十八 年 一 月

小型之寬頻一百八十度混合式耦合器及其應用於寬頻耦合器與濾波器之設計

A Compact Wideband 180$^\text{o}$ Hybrid Coupler and Its Applications to Wideband Coupler and Bandpass Filter Designs

研究生：紀鈞翔　　　　　　　　　Student: Chun-Hsiang Chi

指導教授：張志揚　博士　　　　　Advisor: Dr. Chi-Yang Chang

國立交通大學

電信工程學系

博士論文

A Dissertation
Submitted to Institute of Communication Engineering
College of Electrical and Computer Engineering
National Chiao Tung University
in Partial Fulfillment of the Requirements
for the Degree of Doctor of Philosophy
in
Communication Engineering
Hsinchu, Taiwan

2009 年 1 月

小型之寬頻一百八十度混合式耦合器及其應用於寬頻耦合器與濾波器之設計

研究生：紀鈞翔　　　　　　　　　　指導教授：張志揚博士

國立交通大學

電信工程學系

摘要

　　本論文主要研究小型之寬頻一百八十度混合式耦合器以及其應用，在第一部份，介紹步階式寬頻一百八十度混合式環形耦合器，其新型的寬頻一百八十度相位移相器以混合共平面帶線/指插式共平面帶線來實現，由於結合步階阻抗架構及寬頻的相位反轉器，此提出的混合式耦合器不僅尺寸小、寬頻且擁有卓越的性能，在第二部分，提出利用垂直安置基板耦合器的寬頻多節式一百八十度混合式耦合器，基於變形的理想單節式混合式耦合器(內含理想相位反轉器的一百八十度混合式耦合器)，多節的一百八十度混合式耦合器可藉由適當的串接單節的混合式耦合器來實現，相較於傳統的二分之三波長岔路環，此兩節式的混合式耦合器頻寬寬、尺寸小且容易達到高比例的能量分流。最後，介紹藉由串接兩個步階式一百八十度混合式耦合器來實現擁有寬的上止帶之寬頻帶通濾波器。上述電路的分析過程皆有詳細的說明，也提供設計方程式及設計曲線，因此，我們可以系統化的設計這些電路。

A Compact Wideband 180$^\text{o}$ Hybrid Coupler and Its Applications to Wideband Coupler and Bandpass Filter Designs

Student：Chun-Hsiang Chi   Advisor：Dr. Chi-Yang Chang

Department of Communication Engineering

National Chiao Tung University

Abstract

This dissertation presents the research and application of the compact wideband 180^0 hybrid coupler. In the first part, a stepped-impedance wideband 180^0 hybrid ring coupler with a novel wideband 180^0 phase-shifter implemented by the hybrid CPS/interdigital CPS structure is introduced. Due to the combination of the stepped-impedance structure and a wideband phase inverter, the proposed hybrid coupler achieves size reduction, wide bandwidth, and excellent phase and amplitude performances. In the second part, wideband multi-section 180^0 hybrid couplers using the vertically installed planar (VIP) coupler are proposed. On the basis of the reconfigured ideal single-section 180^0 hybrid coupler (the 180^0 hybrid coupler with an ideal phase inverter), the multi-section 180^0 hybrid rings can be realized by properly cascading of the single-section 180^0 hybrid coupler. Compared to the conventional 3/2 λ 180^0 hybrid ring, the two-section hybrid rings exhibit wide bandwidth, size reduction, and easily achievable high power-division ratios. Finally, a wideband bandpass filter with wide upper stopband is presented by cascading two stepped-impedance 180^0 hybrid couplers. Analysis procedures of above-mentioned circuits are described in detail. Also, design equations and design curves are presented. Therefore, we can systematically design these circuits.

誌謝

鈞翔

2009 年 1 月於新竹

Contents

List of Tables

List of Figures

Chapter 1

Introduction

The 180^0 hybrid ring coupler is a fundamental component in microwave circuit applications. Conventionally, a rat-race hybrid consists of three $\lambda/4$ line sections and a $3\lambda/4$ line section as shown in Fig. 1-1. A signal applied to port 1 will be split into two in-phase signal at ports 3 and 4, and port 2 will be isolated. A signal applied to port 2 will be split into two out-of-phase signal at ports 3 and 4, and port 1 will be isolated. It can be used as an 180^0-out-of-phase or in-phase power divider with isolated output ports. Due to these characteristics, the 180^0 hybrid coupler is widely used in balanced mixers, push-pull amplifiers, phase shifters, and feeding networks of antenna arrays.

Recently, a wideband bandpass filter is an important issue in the development of the wideband communication systems. In the design of the wideband filter, two major issues must be considered. One is the wide bandwidth; the other is the spurious problem. In wideband applications, the filter needs not only wide bandwidth to meet the required large data rate but also wide stopband to suppress harmonics.

In this chapter, we describe the shortcomings of the conventional rat-race hybrid, the challenges in the design of the wideband bandpass filter, previous works for rat-race hybrids and wideband bandpass filters, and our proposals.
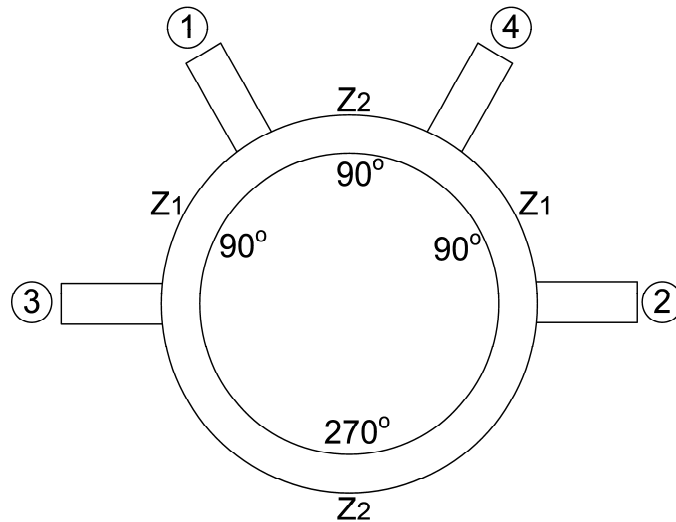
Fig. 1-1. Schematic of the conventional rat-race hybrid.

1.1 Research Motivations

In the conventional rat-race hybrid, the 180^0 phase shifter is implemented by a $\lambda/2$ transmission line and its phase-shift is only 180^0 at the center frequency. Therefore, the conventional hybrid ring using a $3\lambda/4$ line section results in large size and narrow bandwidth. Besides, it requires a quite high impedance line for large power-division ratios.

A wideband bandpass filter with the traditional microstrip half-wavelength parallel coupled-line structure is difficult to manufacture due to very small gaps between coupled strips. Moreover, because of the unequal even- and odd-mode phase velocities, this filter has a first spurious passband at twice of the midband frequency, resulting in poor harmonic suppression.

Most of the proposed circuits are implemented on microstrip structures because microstrip is the most mature and widely used transmission line. However, the realization of a broadband phase inverter using microstrip structure would be a challenge. In recent years, due to advantages of small dispersion, simple realization of short-circuited ends, easy integration with lumped elements and no need for via holes, uniplanar transmission lines such as coplanar waveguide (CPW) and coplanar strip (CPS) have become a competitive alternative to microstrip in many applications.

Therefore, the purpose of this research is to find some approaches to overcome bandwidth and size problems of the rat-race hybrid on microstrip and uniplanar structure. Furthermore, based on theses proposed 180^0 hybrid couplers, several novel

2

bandpass structures are proposed to solve bandwidth and harmonics problems.
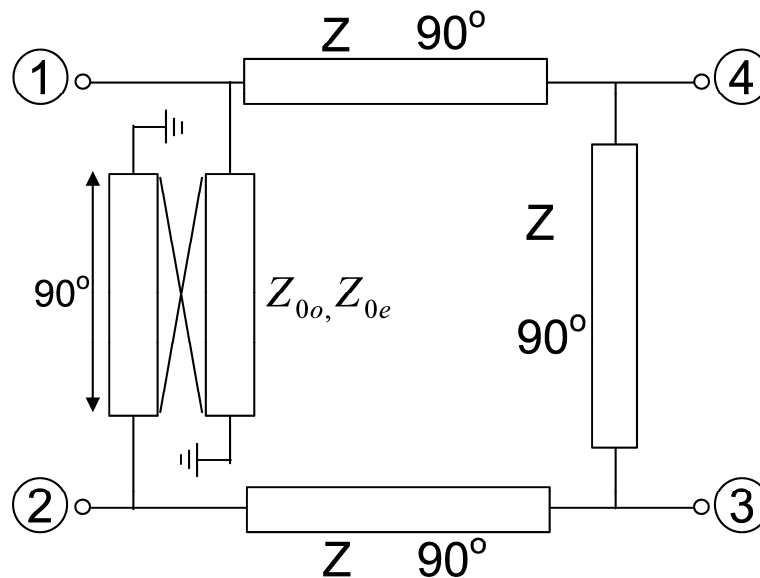
Fig. 1-2. Schematic of the 180^0 hybrid ring coupler proposed by March.

1.2 Literature Survey

In the design of the 180^0 hybrid coupler, many approaches [1]-[5] have been proposed to achieve small size. In [1], [2], using lumped elements were proposed to reduce the size of the hybrid. In [3], a design method for 1.25λ-and 7λ/6-ring 3-dB hybrids using λ/8 and λ/6 section was proposed. Other miniaturized methods were also presented such as folded line [4] and artificial lines [5]. However, in all above-mentioned 180^0 hybrids, it is difficult to simultaneously achieve small size and wide bandwidth. March [6] replaced the 3λ/4 transmission line with an opposing ends short-circuited λ/4 coupled line to increase the bandwidth of the hybrid ring as shown in Fig. 1-2. However, to implement this hybrid ring requires extremely tight coupled lines. A reduced-size rat-race coupler of length 19λ/18 has been developed in [7]. In [8], a lumped-element left-handed transmission line was used to realize the hybrid ring. The 3λ/4 section of the rat-race has been replaced with a λ/4 section and various forms of wideband phase inverters [9]-[16].

A theory of cascading of several quarter-wave transmission-line sections to each I/O port of an ideal 180^0 hybrid ring for bandwidth improvement has been proposed by Rehnmark [17]. Chang et al. [18] have proposed a method to implement the hybrid

ring proposed in [17]. However, to implement these hybrid rings requires extremely low and/or high impedance lines or extremely tight coupled lines especially for large power-division ratio situations. To reduce the impedance values, the $3\lambda/4$ line section of the hybrid ring can be split into three $\lambda/4$ lines [19]. However, the required high impedance values still increase with power-division ratios. Therefore, the realizable highest and/or lowest impedance values limit the achievable power-division ratios of those hybrid rings proposed in [1]-[19].

The 90^0 branch-line coupler [20] realized with a multi-section structure for bandwidth enhancement is well known. The multi-section 180^0 hybrid ring was first proposed by Ang et al. [21] to achieve broad bandwidth and high power-division ratios. However, because each single-section unit in [21] was based on the conventional hybrid ring coupler with the narrow-band phase inverter, the amplitude and the phase performances of two output ports cannot achieve broad bandwidth simultaneously. Therefore, in [21], only conditions at the center frequency are derived and the responses other than center frequency have not been discussed analytically. In addition, the bandwidth of the hybrid ring will dramatically decrease with increasing of power-division ratios.

In the design of the wideband bandpass filter, based on the insertion loss method [22], a wideband bandpass filter function of Chebyshev type can be easily synthesized. However, to realize a wideband bandpass filter with the conventional microstrip half-wavelength parallel coupled-line structure, very small gaps between coupled strips are required to achieve a tight coupling. This may cause some difficulties in the fabrication processes. Moreover, due to the unequal even- and odd-mode phase velocities, this filter has a first spurious passband at $2f_0$, resulting in poor harmonic suppression. To improve bandwidth performance, several methods [23]-[34] have been proposed. In [23], a bandpass filter with increased bandwidth can be obtained from resonator coupling enhancement with the three-line coupling structure was reported. Another method for coupling enhancement using apertures etched in the microstrip ground plane was described in [24]. In [25], a cascade of two cascadable 180° hybrid ring couplers could form a wideband bandpass filter. In [26]-[31], a multiple-mode resonator (MMR) is used to construct a wideband bandpass filter.

In recent years, the ring resonators are utilized to form bandpass filters with the

wide passband. In [32], bandpass filter based on the bandstop filter uses two tuning stubs to construct a wideband passband. A microstrip ring bandpass filter with dual stopbands below 3.1 GHz and above 10.6 GHz was built up in [33].

In [34], a composite UWB filter is realized by cascading lowpass and highpass filters together or embedding one into the other. However, most of the above-mentioned filters show narrow upper stopband performance and some of them even show notch-like upper stopband response. Therefore, it is still a challenge to design a single filter having wide passband and broad upper stopband characteristics simultaneously.

1.3 Contribution

In this dissertation, we propose a novel wideband 180^0 phase shifter using the CPS/interdigital CPS structure to realize the stepped-impedance 180^0 hybrid coupler. Extremely high impedances and low impedances can be implemented by CPS and interdigital CPS respectively. Due to the large high- to low-impedance ratio, the size of this 180^0 hybrid coupler can be reduced significantly. Also, a reconfigured 180^0 hybrid coupler using the VIP coupler is presented and fabricated by microstrip structure. This 180^0 hybrid coupler with two output ports on the same side is convenient for the applications such as balanced-mixer, push-pull amplifier, etc. Based on this cascadable 180^0 hybrid coupler, the multi-section 180^0 hybrid couplers are proposed to exhibit high power-division ratios and wide bandwidth. Furthermore, we propose a novel bandpass filter structure using multi-section 180^0 hybrid couplers to achieve broad bandwidth and wide upper stopband performance.

1.4 Organization of the Dissertation
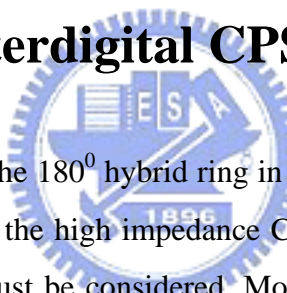
In chapter 2, a novel wideband 180^0 phase shifter using CPS/interdigital CPS structure is proposed to realize the compact wideband 180^0 hybrid coupler. Design equations for stepped-impedance lines and design curves for CPS/interdigital CPS lines are also presented. Chapter 3 describes a single-section cascadable 180^0 hybrid coupler is realized by vertically installed planar (VIP) coupler for size reduction and bandwidth enhancement. Then, based on this single-section cascadable 180^0 hybrid coupler, a two-section cascadable 180^0 hybrid coupler for larger bandwidth and

power- power-division ratios is proposed. Furthermore, the analysis procedures are described in detail for these hybrid couplers. The coupled line using VIP structure is also discussed in this chapter. Chapter 4 presents several novel wideband bandpass filter structures by cascading two 180^0 hybrid couplers. The design methods are also given in this chapter. Chapter 5 gives the conclusion.

Chapter 2

A Compact Wideband 180^0 Hybrid Coupler Using a Novel Interdigital CPS Phase Inverter

In this chapter, we modify the 180^0 hybrid ring in [9] where the phase inverter was implemented by 180^0 twist of the high impedance CPS as shown in Fig. 2-1 and the parasitic effect of the twist must be considered. More importantly, the design of the hybrid ring in [9] was mostly try-and-error using EM simulator. Therefore, we propose the 180^0 hybrid ring coupler with an wideband phase inverter as shown in Fig. 2-2 where three λ/4 line sections and one λ/4 line section cascading an ideal phase inverter are realized by the configurations in Fig. 2-3(a) and (b) respectively. Note that physical dimensions in Fig. 2-3(a) and (b) have the same dimensions so that the design curves in this chapter are valid for both cases. Also, simple design equations for designing of stepped-impedance line are provided. The method described in this chapter can systematically design a hybrid ring with much better performance than that of [9].
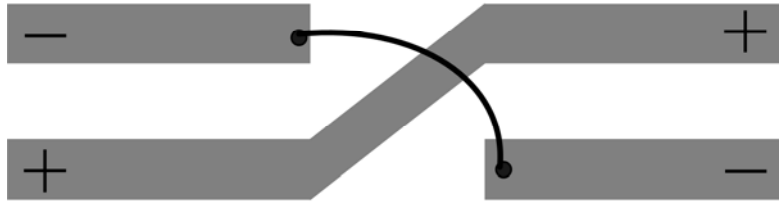
Fig.2-1. Configuration of the wideband phase inverter realized with CPS.
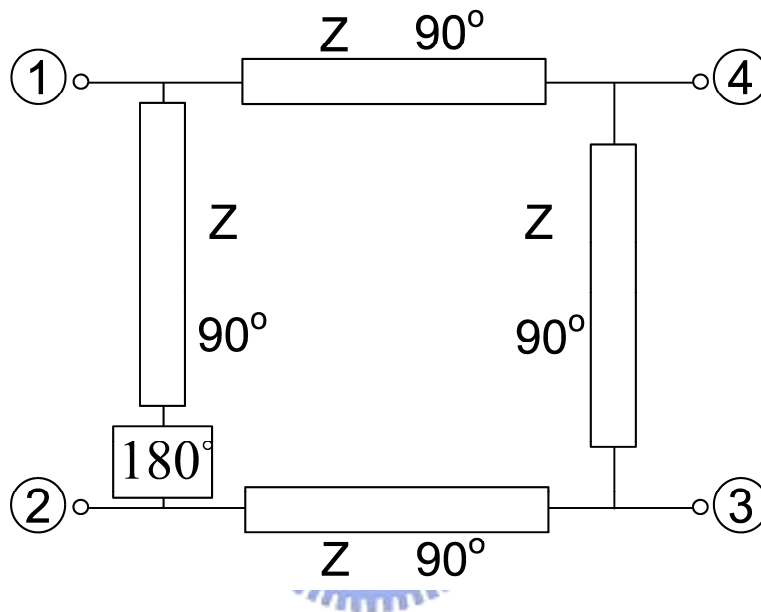
Fig. 2-2. Schematic of the 180^0 hybrid ring with an ideal 180^0 phase inverter.

(a)

(b)

Fig. 2-3. Proposed configurations of the stepped-impedance 180^0 hybrid ring coupler using interdigital CPS (a) $\lambda/4$ line section (b) $\lambda/4$ line section with a wideband phase inverter.

$$Z \quad 90^{\circ}$$

(a)

$$Z_L \ \theta_L \qquad Z_H \ \theta_H \qquad Z_L \ \theta_L$$

(b)
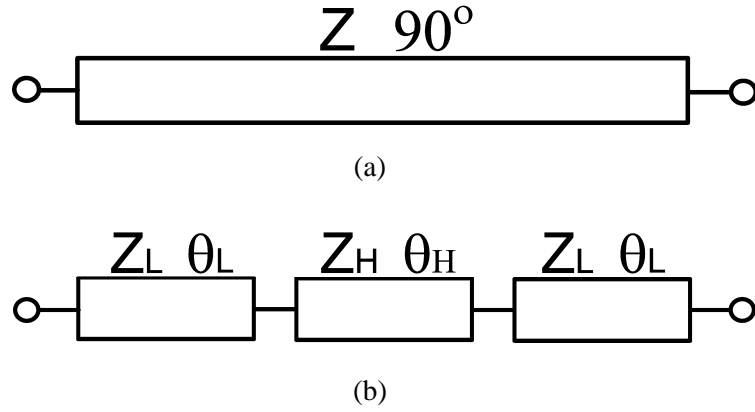
Fig. 2-4. (a) Quarter-wave transmission line (b) Stepped-impedance circuit equivalent to a quarter-wave transmission line

2-1 Analysis of the stepped-impedance line section

The characteristic impedance Z of the hybrid ring corresponding to the specific return loss can be determined by [17]. A quarter-wave transmission line of impedance Z is shown in Fig. 2-4(a) and it serves as a basic building block of the proposed hybrid ring. Its ABCD matrix is given by

$$\begin{bmatrix} A & B \\ C & D \end{bmatrix} = \begin{bmatrix} 0 & jZ \\ \dfrac{j}{Z} & 0 \end{bmatrix}. \tag{2-1}$$

The quarter-wave transmission line can be replaced by a stepped-impedance structure shown in Fig. 2-4(b) where Z_H and Z_L are the characteristic impedances of the cascaded sections and θ_H and θ_L are the corresponding electrical lengths. By choosing $Z_H > Z_L$, the overall electrical length of the stepped-impedance section can be shorter than 90^0. The ABCD matrix of the stepped-impedance section shown in Fig. 2-4(b) is given by

$$\begin{bmatrix} A & B \\ C & D \end{bmatrix} = \begin{bmatrix} \cos\theta_L & jZ_L \sin\theta_L \\ j\dfrac{\sin\theta_L}{Z_L} & \cos\theta_L \end{bmatrix} \bullet \begin{bmatrix} \cos\theta_H & jZ_H \sin\theta_H \\ j\dfrac{\sin\theta_H}{Z_H} & \cos\theta_H \end{bmatrix} \bullet \begin{bmatrix} \cos\theta_L & jZ_L \sin\theta_L \\ j\dfrac{\sin\theta_L}{Z_L} & \cos\theta_L \end{bmatrix}$$

which gives

$$A = \frac{[Z_H Z_L \cos\theta_H \cos 2\theta_L - (Z_H^{\ 2} + Z_L^{\ 2})\cos\theta_L \sin\theta_H \sin\theta_L]}{Z_H Z_L}$$

9

$$B = \frac{j[Z_H^2 \cos^2\theta_L \sin\theta_H + Z_L(-Z_L \sin\theta_H \sin^2\theta_L + Z_H \cos\theta_H \sin 2\theta_L)]}{Z_H}$$

$$C = \frac{j[Z_L^2 \cos^2\theta_L \sin\theta_H + Z_H(-Z_H \sin\theta_H \sin^2\theta_L + Z_L \cos\theta_H \sin 2\theta_L)]}{Z_H Z_L^2}$$

$$D = \frac{[Z_H Z_L \cos\theta_H \cos 2\theta_L - (Z_H^2 + Z_L^2)\cos\theta_L \sin\theta_H \sin\theta_L]}{Z_H Z_L} \tag{2-2}$$

Equating the ABCD matrix of the quarter-wave transmission line and the stepped-impedance structure shown in Fig. 2-4, we have

$$\frac{Z_H Z_L \cos\theta_H \cos 2\theta_L - (Z_H^2 + Z_L^2)\cos\theta_L \sin\theta_H \sin\theta_L}{Z_H Z_L} = 0. \tag{2-3}$$

$$\frac{Z_H^2 \cos^2\theta_L \sin\theta_H + Z_L(-Z_L \sin\theta_H \sin^2\theta_L + Z_H \cos\theta_H \sin 2\theta_L)}{Z_H} - Z = 0. \tag{2-4}$$

$$\frac{Z_L^2 \cos^2\theta_L \sin\theta_H + Z_H(-Z_H \sin\theta_H \sin^2\theta_L + Z_L \cos\theta_H \sin 2\theta_L)}{Z_H Z_L^2} - \frac{1}{Z} = 0. \tag{2-5}$$

2-2 Design steps of the proposed 180[0] hybrid ring coupler

The first step to implement the proposed 180[0] hybrid ring coupler is to specify the required return loss. The next step is to replace each line section in Fig. 2-2 by the stepped-impedance structure. Followings show the procedures. First, arbitrary choose the θ_H and θ_L and then use (2-3)-(2-5) to find Z_H and Z_L. Second, check the obtained Z_H and Z_L to be realizable or not, if not, redo the first step again. Finally, fine-tuning the obtained circuit parameters might be required to optimize the circuit performance. In this work, the 180[0] hybrid ring coupler with 15-dB return loss is designed as an example and the optimized circuit parameters are shown in Table 2-1.

TABLE 2-1

Parameters of the stepped-impedance hybrid ring

	Z_H (Ω)	Z_L (Ω)	θ_H (Degree)	θ_L (Degree)
λ/4, Z=59Ω	184	22	15.2	16.3

10
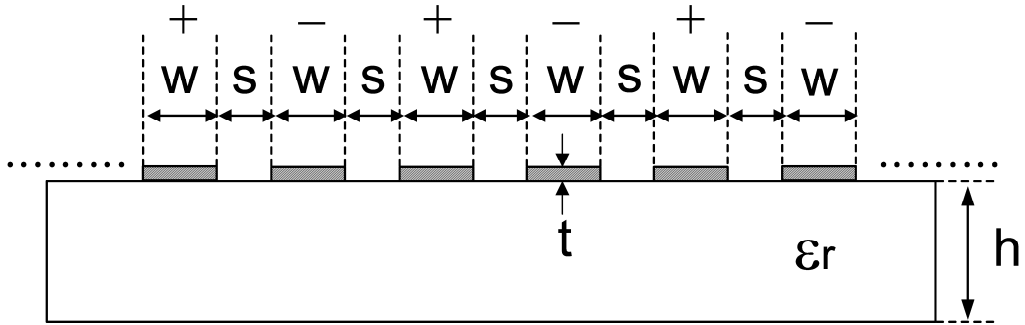
Fig. 2-5. Cross-sectional view of the interdigital CPS with N=3.

2-3 Realization and measurement

From [35], we know that the length of a stepped-impedance line can be significantly reduced with larger high- to low-impedance ratios. However, to realize such high and low impedances simultaneously would be a challenge. Fortunately, this can be solved by using CPS (high impedances) and interdigital CPS (low impedances). The cross-sectional view of the interdigital CPS is shown in Fig. 2-5. Here, N is defined as the number of CPS strip pair (for instance N=2 has 4 strips) and the conductor thickness (t) is assumed to be zero. The proposed hybrid ring coupler is fabricated on an Al_2O_3 alumina substrate with 15-mil thickness (h) and a dielectric constant (ε_r) of 9.8. It is designed to operate at the center frequency of 2 GHz.

Fig. 2-6 shows the computed characteristic impedance and effective dielectric constant of CPS as a function of the gap width with the strip width as a parameter. Fig. 2-7 indicates the computed characteristic impedance and effective dielectric constant of interdigital CPS as a function of the gap width with the number of CPS strip pair as a parameter. It can be found that extremely high impedances can be obtained by conventional CPS with large S and small W and extremely low impedances can be implemented by interdigital CPS with large N, small S, and large W. Using the design curves in Fig. 2-6 and Fig. 2-7, parameters of each line section corresponding to Table 2-1 can be obtained. In this design, we choose N=3 and the parameters of each line section are listed in Table 2-2. Fig. 2-8 shows the simulated magnitudes of S_{11} and S_{21} and the insertion phase difference between two configurations of Fig. 2-3(a) and (b)

with $Z_H=184\Omega$, $\theta_H=15.2^0$, $Z_L=22\Omega$ and $\theta_L=16.3^0$ where the S-parameters are based on 50-Ω port impedances. Note that all mentioned curves are computed by EM simulator Sonnet. It can be seen that insertion phase difference is within 1^0 and S-parameters of them are almost the same. Therefore, the proposed configuration in Fig. 2-3(b) performs perfectly as a wideband phase inverter.
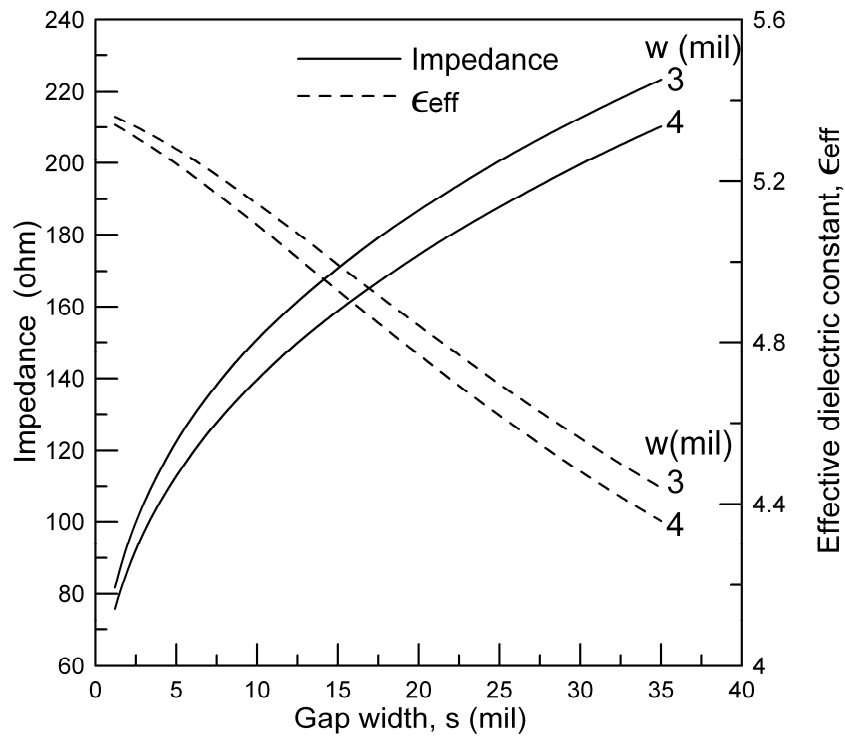
Fig. 2-6. Computed characteristic impedance and effective dielectric constant of CPS as a function of the gap width with the strip width as a parameter, t=0 mil.

TABLE 2-2

CPS and Interdigital CPS parameters of the stepped-impedance hybrid ring

	Line width W (mil)	Gap width S (mil)	Z (Ω)
Interdigital CPS (N=3)	4	1.6	22
CPS	4	24	184
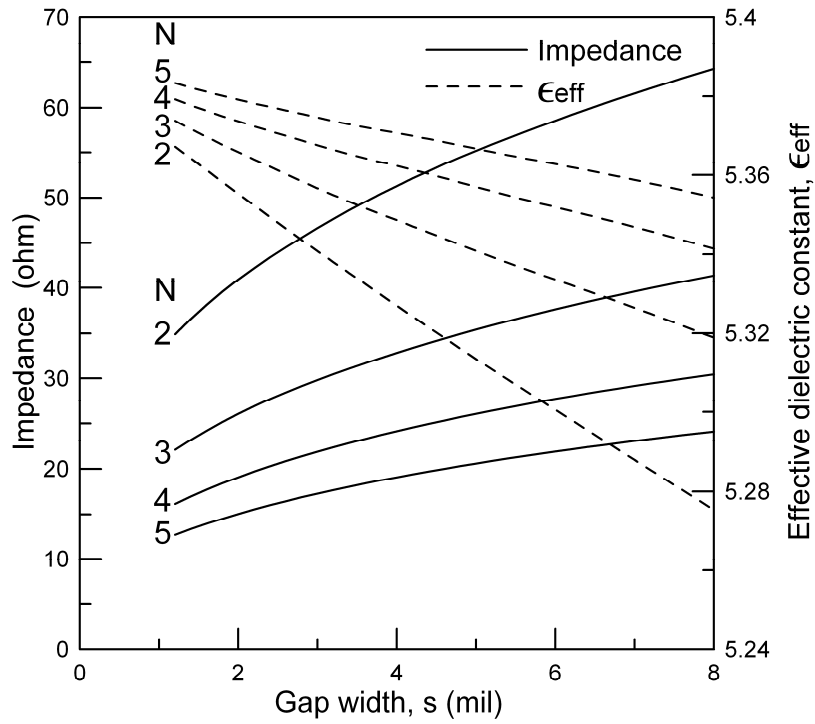
(a)
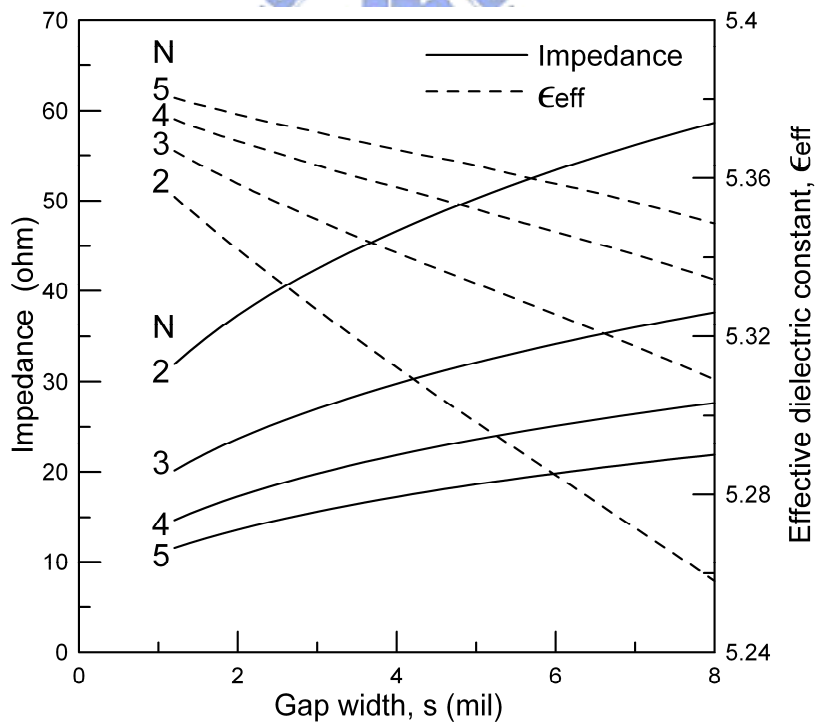
(b)

Fig. 2-7. Computed characteristic impedance and effective dielectric constant of interdigital CPS as a function of the gap width with the number of CPS strip pair as a parameter, t=0 mil (a) w=3 mil (b) w=4 mil.

13
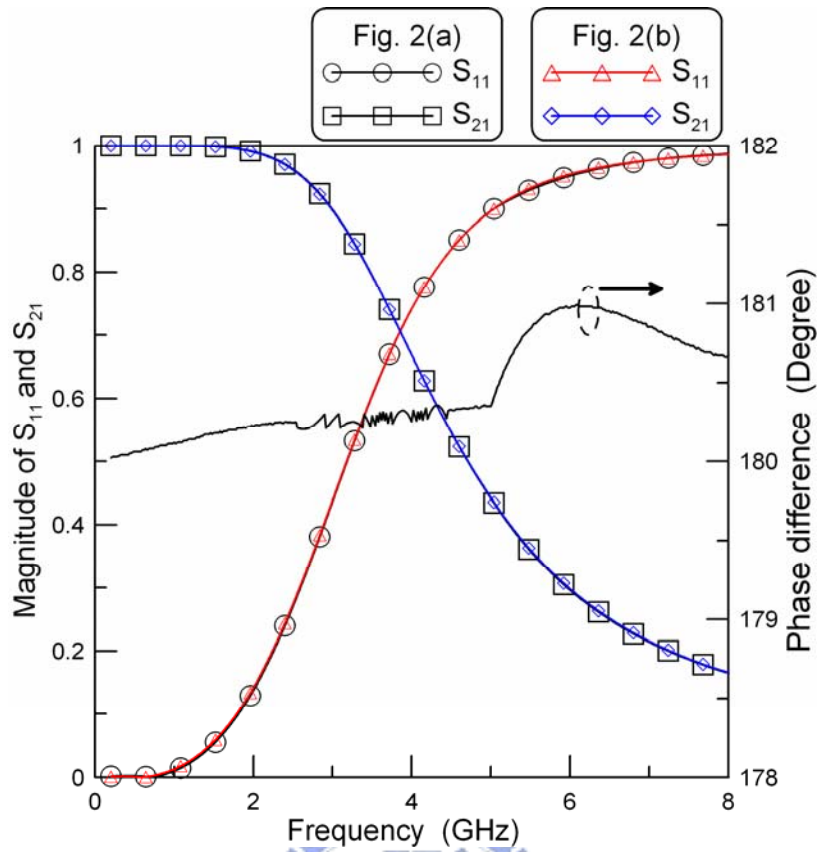
Fig. 2-8. Simulated magnitude of S_{11} and S_{21} and insertion phase difference between two configurations of Fig. 2(a) and (b) with $Z_H=184\Omega$, $\theta_H=15.2^0$, $Z_L=22\Omega$ and $\theta_L=16.3^0$ where the S-parameters are based on 50-Ω port impedances.
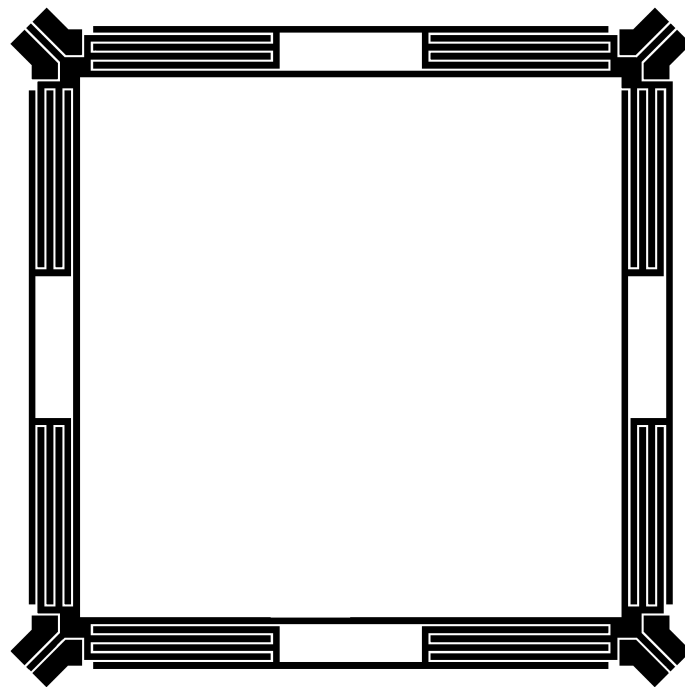
(a)
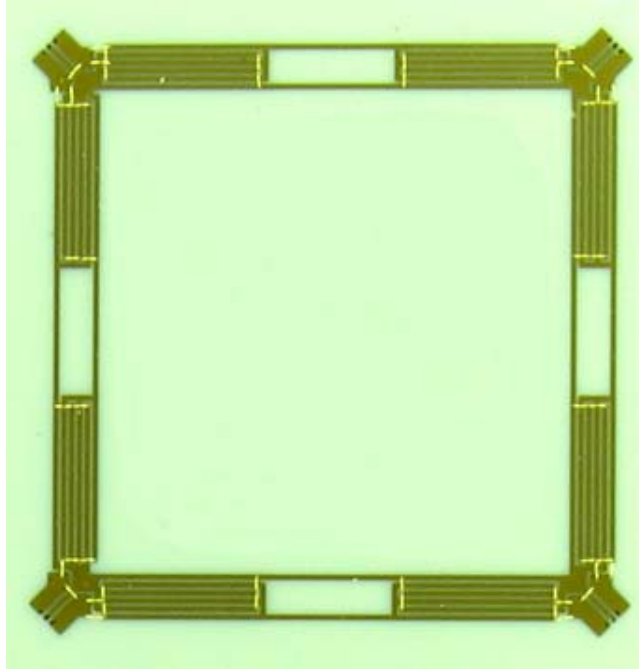
(b)

Fig. 2-9. Fabricated 180^0 hybrid ring coupler (a) Layout (b) Photograph.

The layout and photograph of the fabricated 180^0 hybrid ring coupler are shown in Fig. 2-9. The size of this hybrid is 404 mil $\times$ 404 mil. Fig. 2-10 depicts the measured results of the fabricated hybrid ring coupler and the measured insertion loss is approximately 0.6 dB. The measured return losses are better than 10 dB from 0.98 to 2.93GHz for out-of-phase operation and from 0.97 to 2.96 GHz for in-phase operation, respectively. The measured isolation is better than 30 dB from 0.5 to 4 GHz. The measured amplitude and phase differences are shown in Fig. 2-11. For out-of-phase operation, the amplitude difference is within 0.5 dB from 0.7 to 4 GHz and the phase difference is within 2^0 from 0.5 to 4 GHz. For in-phase operation, the amplitude difference is within 0.5 dB from 0.5 to 4 GHz and the phase difference is within 3^0 from 0.5 to 4 GHz. Fig. 2-12 shows the measured and simulated results from 0 to 20 GHz. The measured performances of the 180^0 hybrid ring coupler are summarized in Table 2-3.

15

(a)
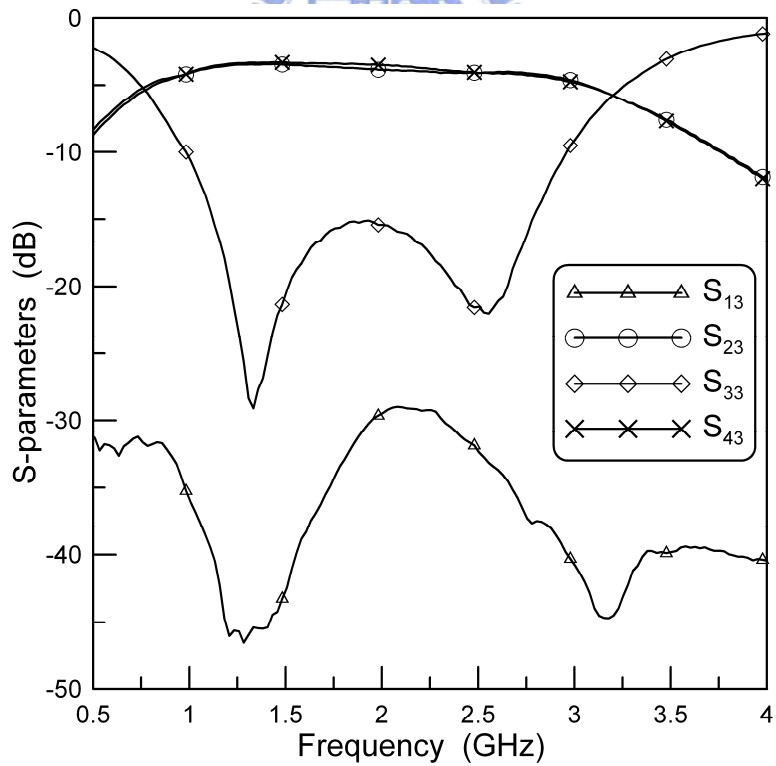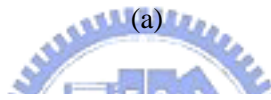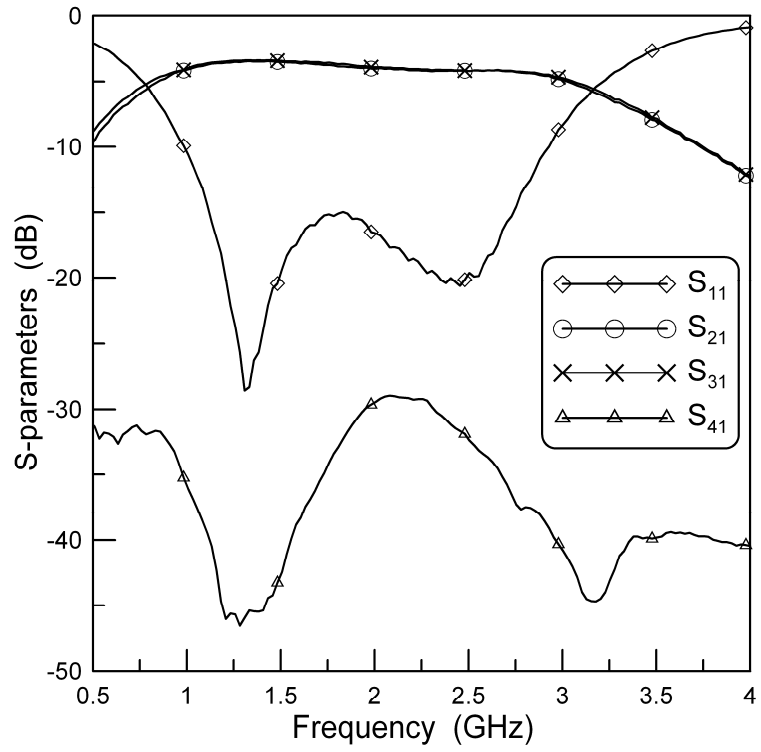
(b)

Fig. 2-10. Measured results of the fabricated 180^{0} hybrid ring coupler (a) Out-of-phase operation (b) In-phase operation
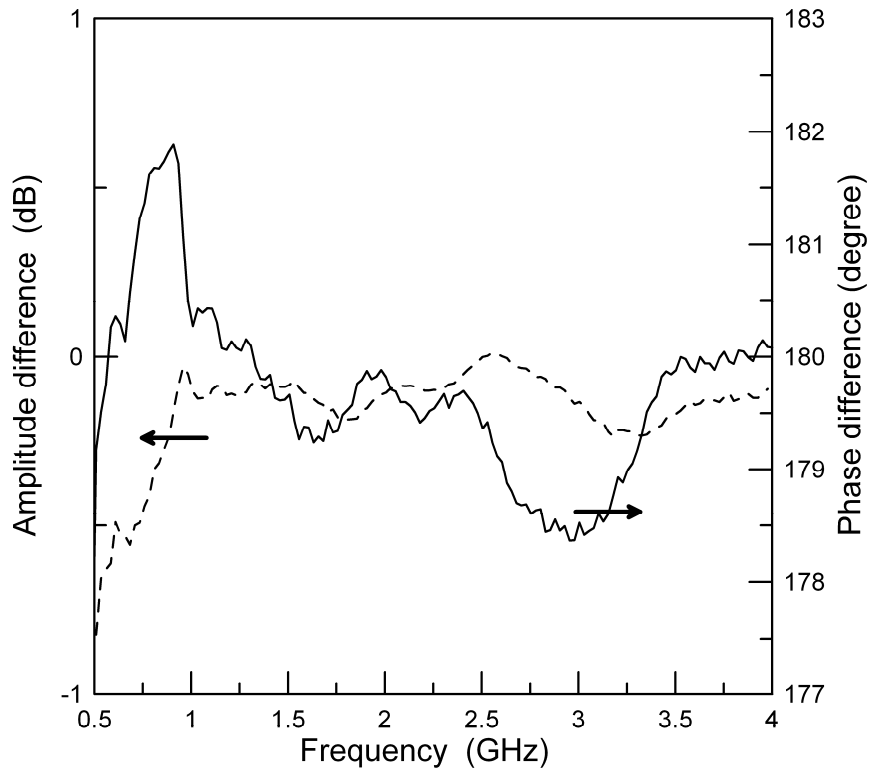
(a)
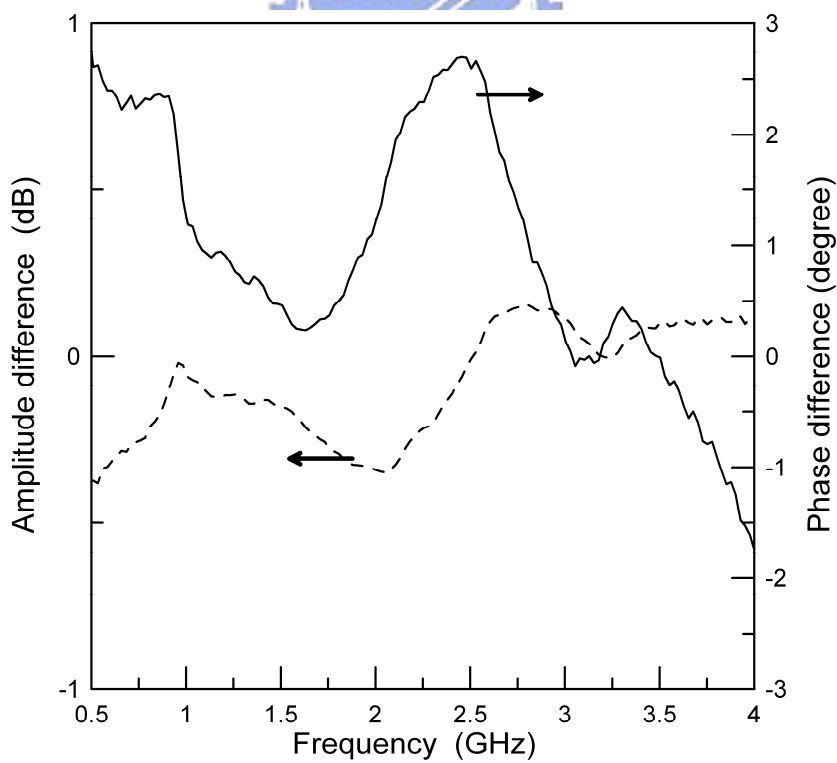
(b)

Fig. 2-11. Measured phase and amplitude differences of the fabricated 180^0 hybrid ring coupler (a) Out-of-phase operation (b) In-phase operation.

17
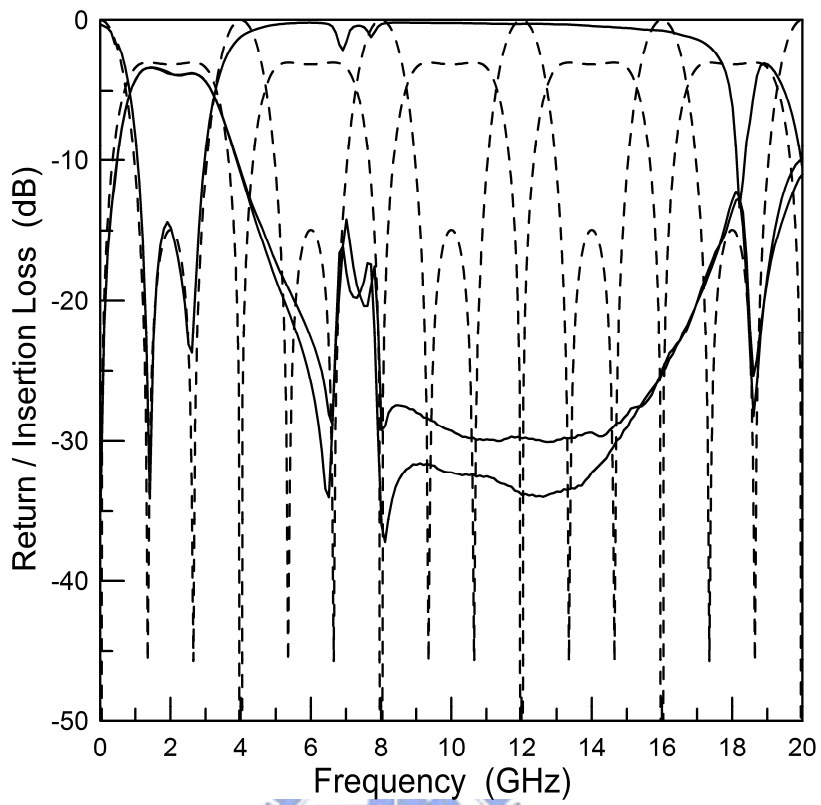
Fig. 2-12. Measured and simulated results from 0 to 20 GHz.

TABLE 2-3

Summary of measured performances of the 180^0 hybrid ring coupler

	Out-of-phase	In-phase
Frequency range [GHz] (RL< -10dB)	0.98~2.93 (97.5%)	
Phase imbalance [Degree]	180 ± 2	0 ± 3
Frequency range [GHz]	$0.5 \sim 4$	
amplitude imbalance [dB]	0 ± 0.4	0 ± 0.5
Frequency range [GHz]	$0.75 \sim 4$	
Frequency range[GHz] Isolation< -30dB	$0.5 \sim 4$	

Chapter 3

Wideband Multi-section 180^0 Hybrid Couplers Using Vertically Installed Planar Couplers

In this chapter, the multi-section 180^0 hybrid rings are proposed to overcome the problems of high power-division ratios and broad bandwidth. The basic building block of the proposed multi-section 180^0 hybrid ring is the reconfigured ideal 180^0 hybrid ring as shown in Fig. 3-1(a) and (b). The proposed single-section hybrid ring can be easily cascaded like the 90^0 branch-line coupler as depicted in Fig. 3-1(c). The reconfiguration proposed in Fig. 3-1(b) also results in size reduction. Furthermore, the hybrid ring in Fig. 3-1(b) with two output ports on the same side is convenient for the applications such as balanced-mixer, push-pull amplifier, etc. Synthesis procedures to realize Chebyshev-response two-section cascaded 180^0 hybrid rings shown in Fig. 3-1(c) with various power-division ratios will be described. The reconfigured single-section 180^0 hybrid ring with a unit element at each port [17], [18] can be cascaded to exhibit extended bandwidth as shown in Fig. 3-2. As an example, the 3-dB two-section hybrid ring with 15-dB return loss yields a bandwidth of 5:1. However, the realization of a broadband phase inverter on microstrip circuits could be a problem. Fortunately, as described in [6] that a short-ended $\lambda/4$ coupled line can provide 270^0 phase-shift and the ratio of the even- and odd-mode impedance of the

19

coupled line determines the bandwidth. The higher even- to odd-mode impedance ratio produces wider bandwidth. As the ratio approaches to an asymptotic value, the short-ended coupled line is equivalent to a $\lambda/4$ line cascaded with an ideal phase inverter. To achieve an enough bandwidth, a very tight coupled line must be implemented. In this chapter, the VIP coupler described in [36] is proposed to implement the very tight coupled lines. With the VIP coupler, the proposed wideband multi-section hybrid rings can be easily implemented by microstrip circuits. Several design examples show that the proposed multi-section 180^0 hybrid rings not only exhibit broad bandwidth but also depict wide range of power-division ratios.

(a)

(b)

(c)
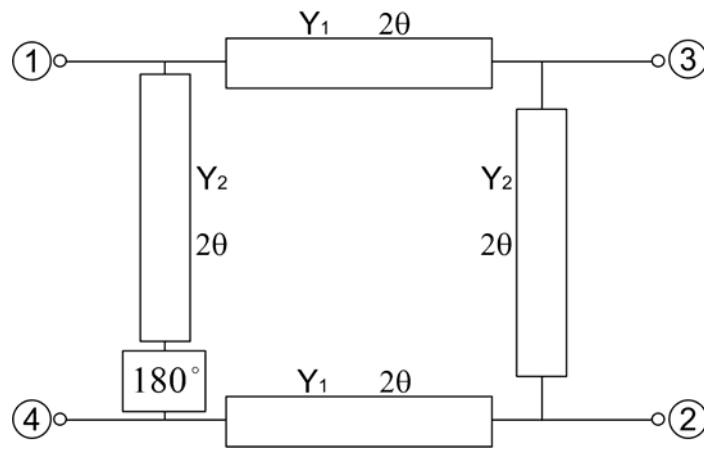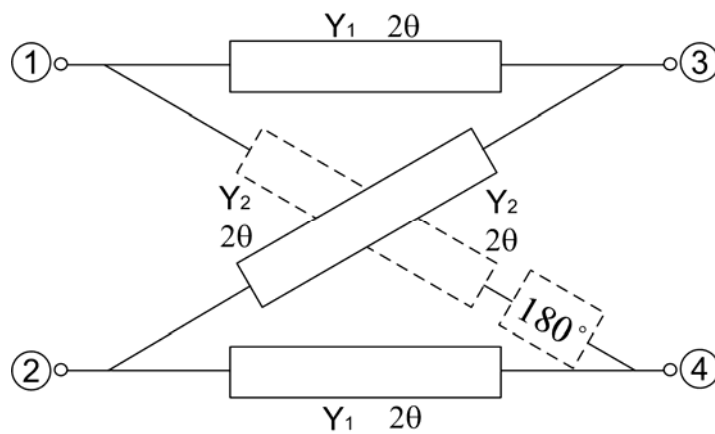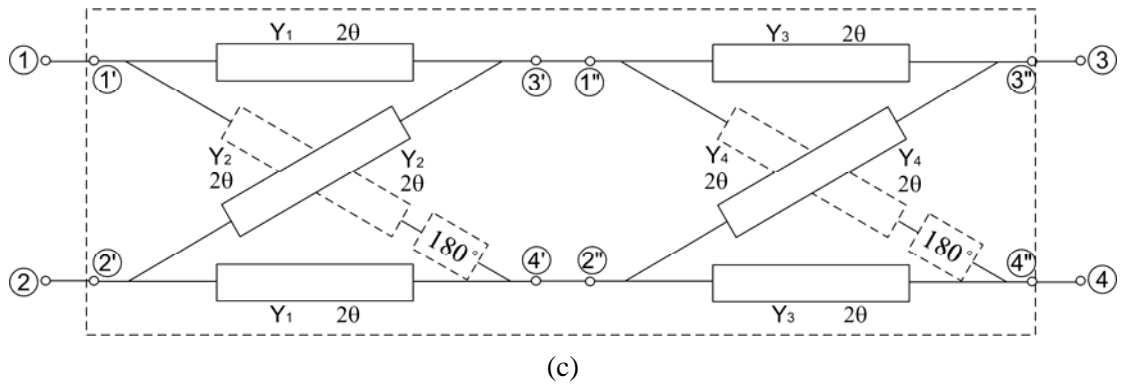
Fig. 3-1. Schematics of hybrid rings using an ideal phase inverter (a) Conventional hybrid ring (b) Reconfigured hybrid ring (c) Proposed two-section hybrid ring.
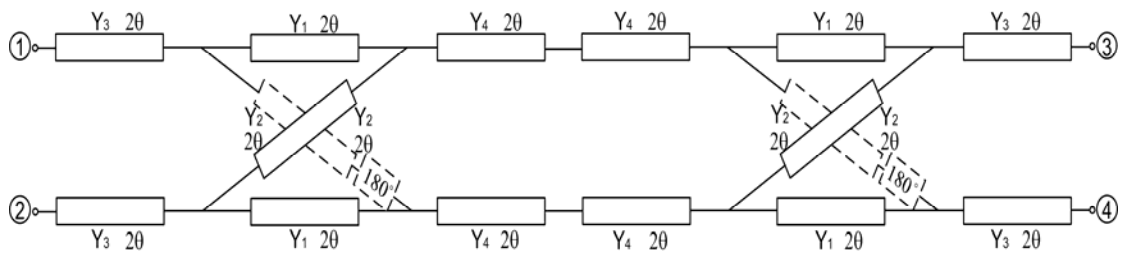
Fig. 3-2. Schematic of the proposed two-section hybrid ring with a unit element at each I/O port.
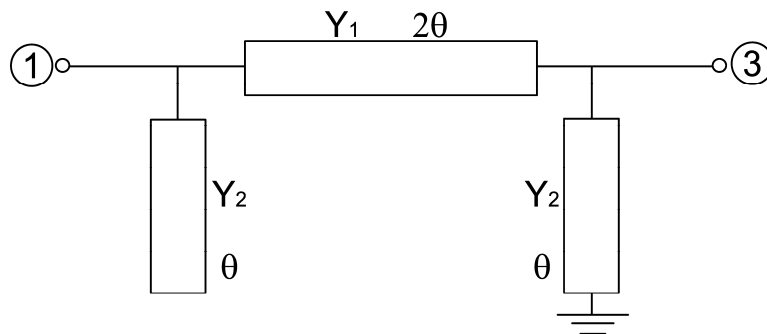
(a)
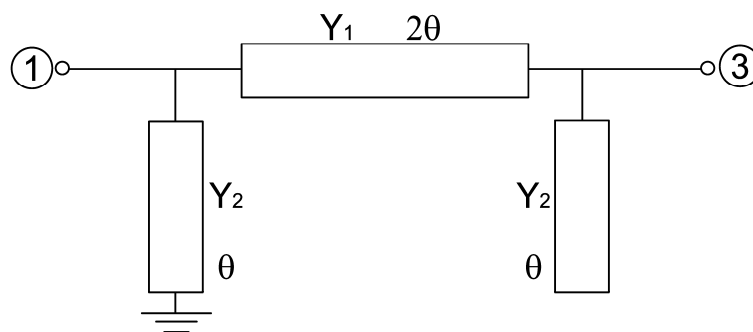
(b)

Fig. 3-3. (a) Even-mode and (b) odd-mode equivalent circuits of the rat-race ring coupler using an ideal phase inverter.

3.1 Theoretical analysis of the two-section hybrid ring

In the reconfigured single-section hybrid ring shown Fig. 3-1(b), the admittance Y_1 and Y_2 are normalized values with respect to system admittance Y_0. Fig. 3-3 shows the even- and odd-mode equivalent circuits of the rat-race ring hybrid using an ideal phase inverter. Using the even- and odd-mode analysis, the ABCD matrices for the even- and odd-mode cascade elements are given by

$$\begin{bmatrix} A_e & B_e \\ C_e & D_e \end{bmatrix} = \frac{1}{(1-t^2)} \begin{bmatrix} A_1(t^2) & tB_0(t^2) \\ \frac{1}{t}C_2(t^2) & D_1(t^2) \end{bmatrix} = \begin{bmatrix} A & B \\ C & D \end{bmatrix}$$

(3-1)

$$\begin{bmatrix} A_o & B_o \\ C_o & D_o \end{bmatrix} = \begin{bmatrix} D_e & B_e \\ C_e & A_e \end{bmatrix} = \begin{bmatrix} D & B \\ C & A \end{bmatrix}$$

(3-2)

where $t = j\tan\theta$ and the subscripts indicate the degree of the polynomials $A(t^2)$, $B(t^2)$, $C(t^2)$, and $D(t^2)$. The reflection and transmission coefficients of the even- and odd-mode cascade elements are

$$\Gamma_e = \frac{(A-D)+(B-C)}{A+B+C+D}$$

$$\Gamma_o = \frac{(D-A)+(B-C)}{A+B+C+D}$$

$$T_e = T_o = \frac{2}{A+B+C+D}$$

(3-3)

Therefore, the S-parameters of the single-section hybrid ring can be expressed as

$$S_{11s} = S_{22s} = \frac{1}{2}(\Gamma_e + \Gamma_o) = \frac{B-C}{A+B+C+D}$$

$$S_{21s} = \frac{1}{2}(T_e - T_o) = 0$$

$$S_{31s} = S_{42s} = \frac{1}{2}(T_e + T_o) = \frac{2}{A+B+C+D}$$

$$S_{32s} = \frac{1}{2}(\Gamma_e - \Gamma_o) = \frac{A-D}{A+B+C+D} = \frac{2(Y_2/Y_1)}{A+B+C+D}$$

$$S_{41s} = \frac{D-A}{A+B+C+D} = \frac{-2(Y_2/Y_1)}{A+B+C+D}$$

(3-4)

The conventional even- and odd- mode analysis method to obtain the S-parameters of the cascaded 90^0 hybrid ring [20] can not be used in this newly proposed two-section hybrid ring shown in Fig. 3-1(c) because the symmetrical planes for even-

and odd-mode excitation are not exist. Here, the multi-port connection method [37] is used. The results at the center frequency are shown as follows:

$$S_{11} = S_{22} = -S_{33} = -S_{44} = \frac{(Y_3^2 + Y_4^2) - (Y_1^2 + Y_2^2)}{Y_1^2 + Y_2^2 + Y_3^2 + Y_4^2}$$

$$S_{21} = 0$$

$$S_{31} = -\frac{2(Y_1Y_3 - Y_2Y_4)}{Y_1^2 + Y_2^2 + Y_3^2 + Y_4^2}$$

$$S_{41} = \frac{2(Y_2Y_3 + Y_1Y_4)}{Y_1^2 + Y_2^2 + Y_3^2 + Y_4^2}$$

$$S_{32} = -\frac{2(Y_2Y_3 + Y_1Y_4)}{Y_1^2 + Y_2^2 + Y_3^2 + Y_4^2}$$

$$S_{42} = -\frac{2(Y_1Y_3 - Y_2Y_4)}{Y_1^2 + Y_2^2 + Y_3^2 + Y_4^2}$$

(3-5)

When $Y_1 = Y_3$ and $Y_2 = Y_4$, all ports can be perfectly matched and the signal incident at the input port will be split between port 3 and port 4. Although all ports can be perfectly matched for the case of $Y_1 = Y_4$ and $Y_2 = Y_3$, a zero dB coupler, which means that no signal can be obtained from one of the output ports, is obtained. Therefore, we concentrate our attention in the case of $Y_1 = Y_3$ and $Y_2 = Y_4$. Because in this case the two-section hybrid ring consists of two identical single-section hybrid rings, the synthesis procedure can be largely simplified. Again, applying the multi-port connection method to (3-4), we can obtain

$$S_{11} = \frac{2[B^2(A + 2C + D) + B(2 + A^2 - 2C^2 + D^2) - C(2 + A^2 + AC + CD + D^2)]}{(A + B + C + D)(A + 2B + D)(A + 2C + D)}$$

$$S_{21} = 0$$

$$S_{31} = -\frac{(A - D)^2 - 4}{(A + 2B + D)(A + 2C + D)} = -\frac{4(Y_2/Y_1)^2 - 4}{(A + 2B + D)(A + 2C + D)}$$

$$S_{41} = -\frac{4(A - D)}{(A + 2B + D)(A + 2C + D)} = -\frac{8(Y_2/Y_1)}{(A + 2B + D)(A + 2C + D)}$$

23

$$S_{32} = \frac{4(A-D)}{(A+2B+D)(A+2C+D)} = \frac{8(Y_2/Y_1)}{(A+2B+D)(A+2C+D)}$$

$$S_{42} = -\frac{(A-D)^2 - 4}{(A+2B+D)(A+2C+D)} = -\frac{4(Y_2/Y_1)^2 - 4}{(A+2B+D)(A+2C+D)}$$

(3-6)

It should be noted that the interchange between Y_1 and Y_2 results in the interchange between the sum port and the delta port. Assuming that the input is matched well in the passband, we have

$$\left|S_{31}\right|^2 + \left|S_{41}\right|^2 \approx 1$$

(3-7)

The output power-division ratio is

$$R = \frac{\left|S_{41}\right|^2}{\left|S_{31}\right|^2} = \left(\frac{2(Y_2/Y_1)}{(Y_2/Y_1)^2 - 1}\right)^2$$

(3-8)

and (3-7) can be written as

$$\left|S_{31}\right|\sqrt{1+R} \approx 1$$

(3-9)

Now, considering the function

$$F = \frac{\left|S_{11}\right|}{\left|S_{31}\right|\sqrt{1+R}}$$

(3-10)

where F is approximately equivalent to the reflection coefficient of the two-section hybrid ring over the passband because the denominator is very close to unity [see (3-9)]. Therefore, the insertion loss function P_L can be shown as follows:

$$P_L = 1 + \left|F\right|^2$$
$$= 1 + \left|\frac{2[B^2(A+2C+D) + B(2+A^2-2C^2+D^2) - C(2+A^2+AC+CD+D^2)]}{\sqrt{1+R}(A+B+C+D)[(A-D)^2-4]}\right|^2$$

(3-11)

As described by Riblet [38], and Carlin and Kohler [39], the insertion loss function of a Chebyshev response has the form

$$P_L = 1 + m^2\{\frac{(1+\sqrt{1-x_c^2})T_n(x/x_c) - (1-\sqrt{1-x_c^2})T_{n-2}(x/x_c)}{2\sqrt{1-x^2}}\}^2$$

(3-12)

where $x = \cos 2\theta$, $x_c = \cos 2\theta_c$, $T_n(x)$ is the Chebyshev polynomial of the first kind of degree n ,and m is the parameter to control the ripple level. Substituting A, B, C, and

24

D in (3-1) into (3-11) and fitting (3-11) to (3-12) with n=3, we obtain

$$\frac{(Y_1+Y_2)(1-Y_1^{\ 2}-Y_2^{\ 2})}{Y_1^{\ 2}\left[\left(\dfrac{Y_2}{Y_1}\right)^2-1\right]\sqrt{1+R}}=m(\frac{2}{x_c}+\frac{\sqrt{1-x_c^{\ 2}}}{x_c})$$

(3-13)

$$\frac{(Y_1+Y_2)(-1+Y_1^{\ 2}+2Y_1Y_2+Y_2^{\ 2})}{Y_1^{\ 2}\left[\left(\dfrac{Y_2}{Y_1}\right)^2-1\right]\sqrt{1+R}}=-m(\frac{2}{x_c^{\ 3}}+\frac{2\sqrt{1-x_c^{\ 2}}}{x_c^{\ 3}})$$

(3-14)

The relationship between m and return loss is

$$RL=10\log(1+1/m^2)\ dB$$

(3-15)

According to (3-8), (3-13), (3-14), and (3-15), the unknown variables Y_1 and Y_2 can be solved numerically. It should be emphasized that there exists two set of solutions. Let us discuss in the following.

Fig. 3-4. Characteristic impedances Z_1, Z_2, and bandwidth versus return loss for the equal-ripple response 3-dB two-section hybrid ring.

Fig. 3-4 shows the plot of characteristic impedances of Z_1, Z_2, and bandwidth versus return loss for the 3-dB two-section hybrid ring shown in Fig. 3-1(c). The 96.3% bandwidth for return loss better than 15dB can be achieved. A similar synthesis procedure can be used to solve the unknown variables for the single-section hybrid ring. Fig. 3-5 shows the plots of characteristic impedances of Z_1, Z_2, and bandwidth versus coupling level, which is defined by the power at coupling port divided by the incident power, for the single- and two-section hybrid rings with 15-dB return loss. It can be seen that, for the single-section hybrid ring, the bandwidth increases with increasing power-division ratios, but the high impedance value of Z_1 limits the realizable power-division ratios to about -10dB. The bandwidth of the two-section hybrid ring decreases with increasing of the power-division ratios but the values of Z_1 and Z_2 are both located in the reasonable range for power-division from as strong as -3dB to weaker than -20dB.

Fig. 3-5. Characteristic impedances Z_1, Z_2, and bandwidth versus coupling level for the single- and two-section hybrid rings with 15-dB equal-ripple return loss.

Fig. 3-6 shows another set of solutions for the two-section hybrid ring. Comparing to the characteristics of the single-section hybrid ring in Fig. 3-5, it depicts a larger bandwidth, but requires a higher Z_1 impedance value. The two-section hybrid ring shown in Fig. 3-2 comprises two single-section units where each unit has a unit element at each I/O port. This two-section hybrid ring can achieve larger bandwidth than above described two-section hybrid ring. However, the analysis method described above is too complicated to obtain similar design equations. Fortunately, values of unknown variables Y_1, Y_2, Y_3, and Y_4 can be obtained by optimization with the known relationship between Y_1 and Y_2. The design curves for a two-section 3-dB hybrid of this type are shown in Fig. 3-7.
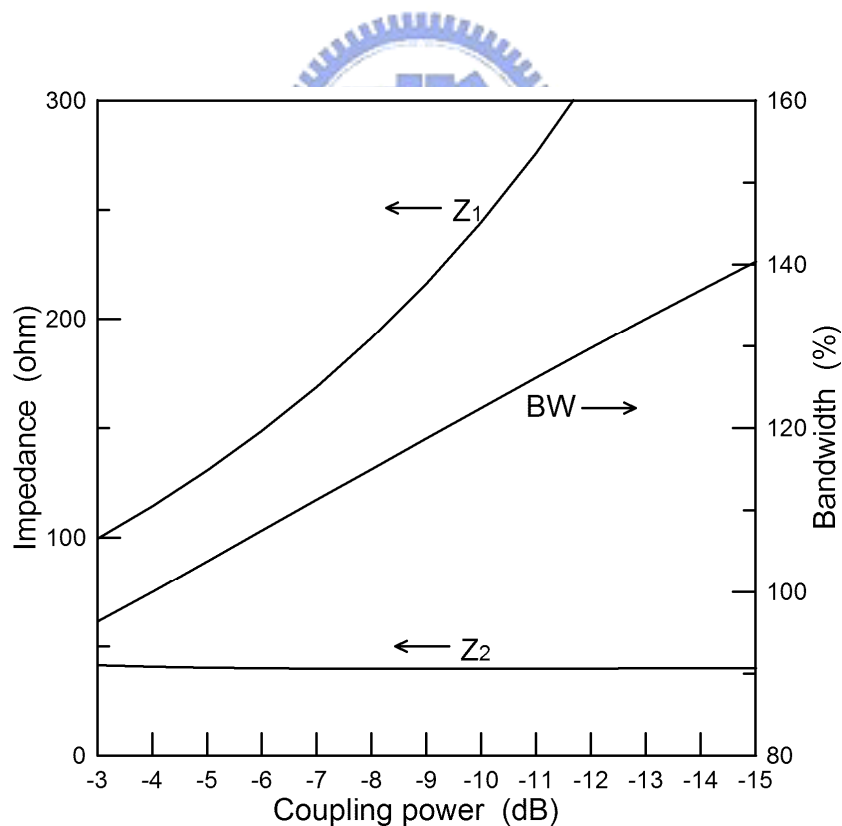
Fig. 3-6. Another set of characteristic impedances Z_1, Z_2, and bandwidth versus coupling level for the two-section hybrid rings with 15-dB equal-ripple return loss.
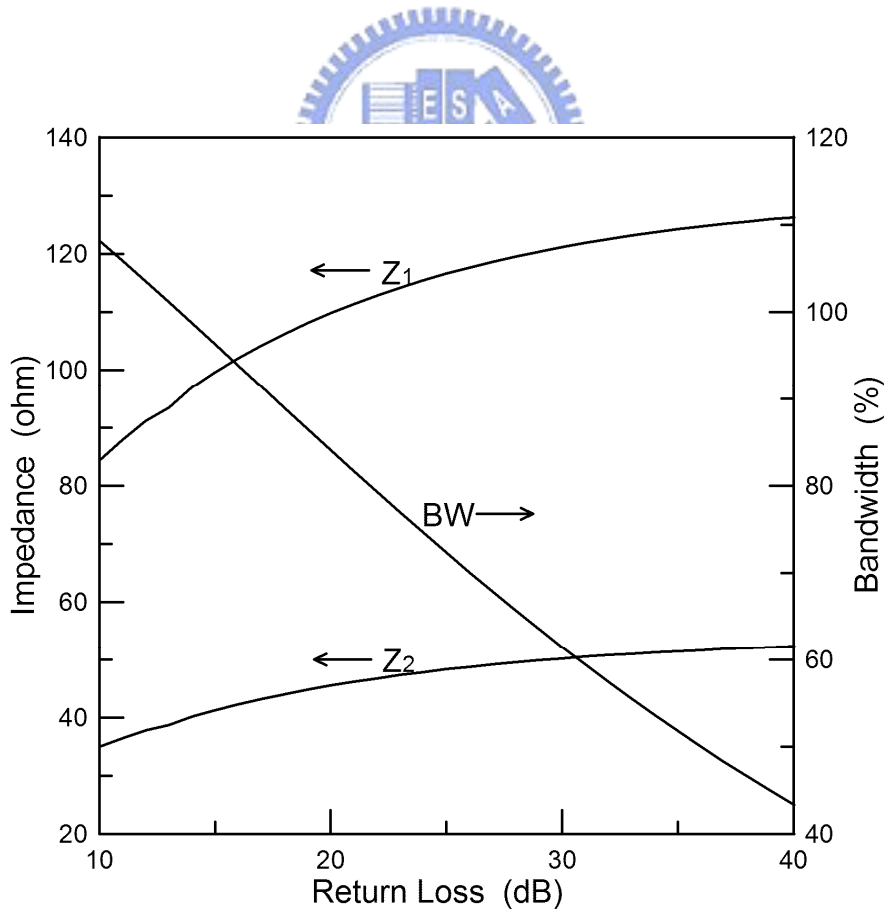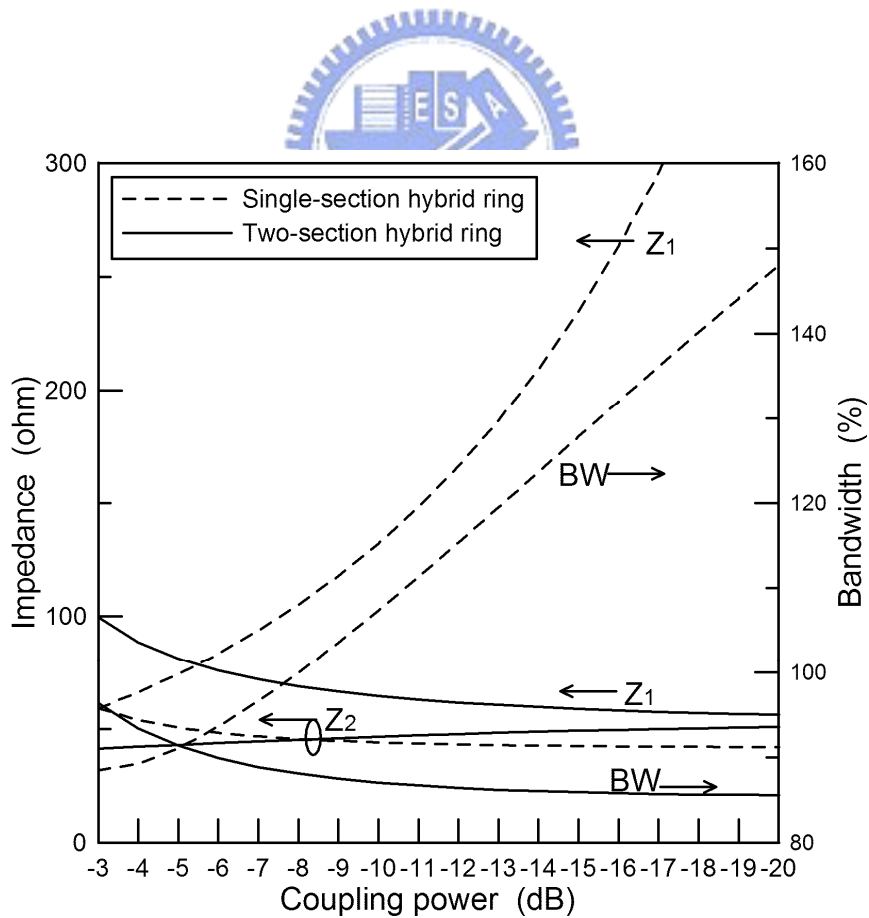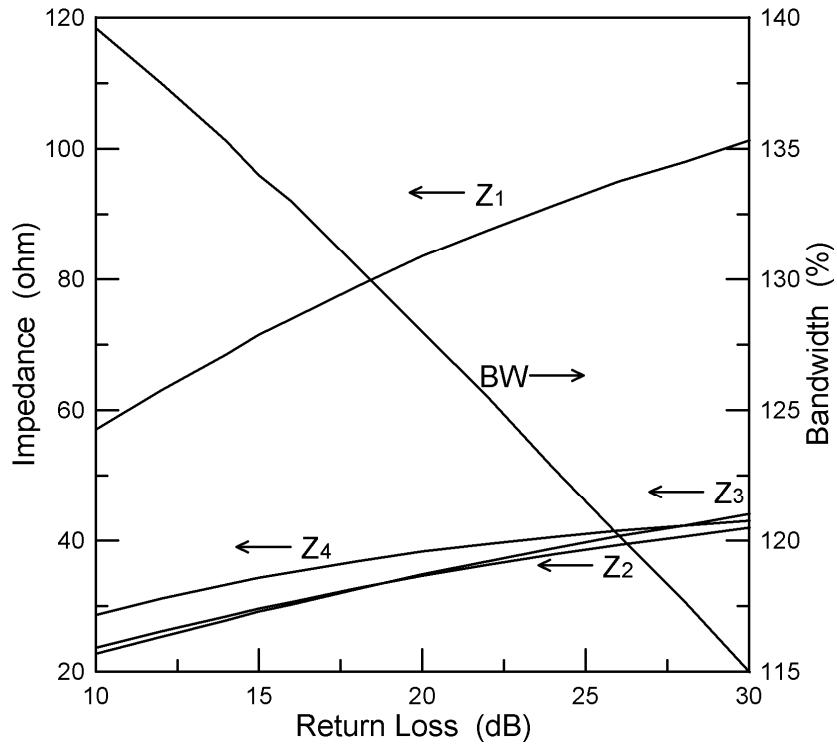
Fig. 3-7. Characteristic impedances Z_1, Z_2, Z_3, Z_4, and bandwidth versus return loss for the equal-ripple response 3-dB two-section hybrid ring with a unit element at each I/O port.
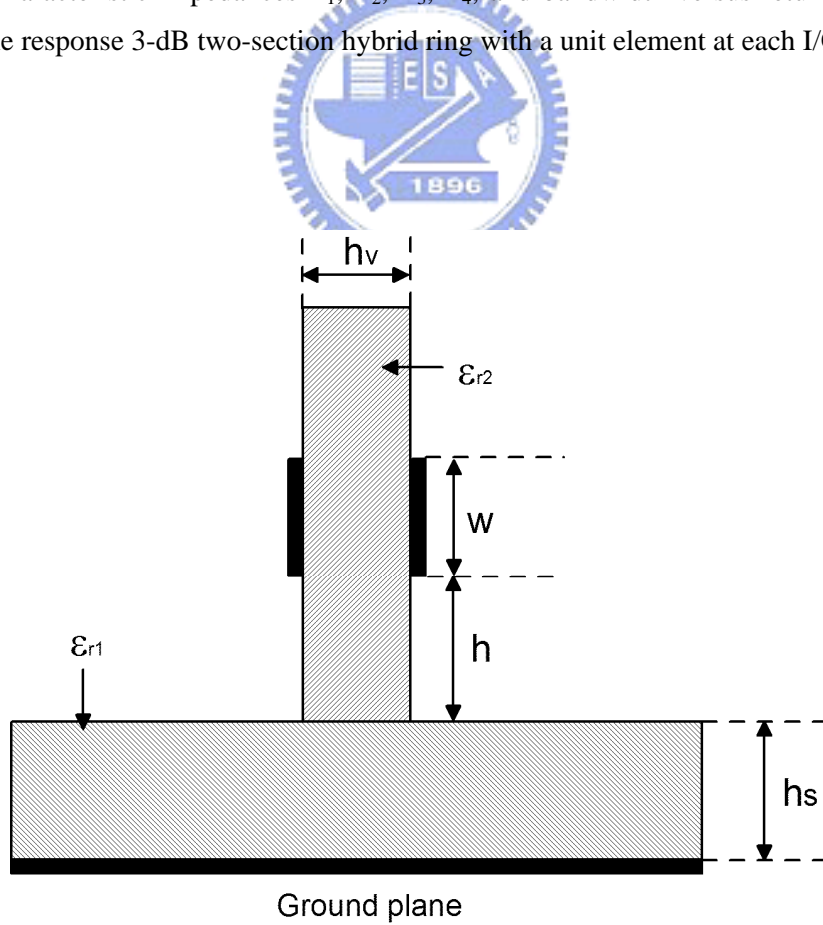
Fig. 3-8. Cross-sectional view of the VIP coupler.

3.2 Characteristics of VIP couplers

Fig. 3-8 shows the cross-sectional view and the parameters of the VIP coupler. Coupling coefficients can be readily controlled by changing the dielectric constants or the thicknesses of the substrates or the height h and width w of the coupler. Therefore, the newly added vertical substrate can significantly increase the freedom of design. From [36], we know that the electric field is mainly confined in the vertical substrate for odd-mode excitation and in air and main substrate for even-mode excitation.

The equivalent circuit of a short-ended coupled line is shown in Fig. 3-9 where Z_{0e} and Z_{0o} are the even- and odd-mode characteristic impedances and θ is the electrical length of the coupled line. When $\theta=90^0$, the two shunt shorted stubs of the characteristic impedance Z_{0e} are open-circuited. Therefore, at the center frequency, the short-ended coupled line is reduced to a $\lambda/4$ transmission line of characteristic impedance $2Z_{0e}Z_{0o}/(Z_{0e}-Z_{0o})$ cascaded with an ideal phase inverter. It should be emphasized that previously described theory is based on an ideal single-section 180^0 hybrid ring. However, the two shunt shorted stubs in Fig. 3-9 are only open-circuited at the center frequency. Out of center frequency, the influence of this shunt shorted stub decreases as the value of Z_{0e} increases. Until Z_{0e} approaches to infinity, the short-ended coupled line is equivalent to the phase inverting arm required in an ideal single-section 180^0 hybrid ring. To obtain higher Z_{0e}, we can increase the height h of the coupler. Comparing Fig. 3-1(b) and Fig. 3-9, it can be found that the value of Z_{0o} is closed to $Z_2/2$ as long as Z_{0e} is much higher than Z_{0o}. The VIP coupler can not only realize low values of Z_{0o} but also implement high values of Z_{0e}. Here, the main circuit is fabricated on a RO4003 substrate with 20-mil thickness (h_s) and a dielectric constant (ε_{r1}) of 3.38 and the VIP coupler is implemented on same RO4003 substrate with 8-mil thickness (h_v) and same dielectric constant (ε_{r2}) of 3.38. The characteristic impedances for even- and odd-modes of the VIP couplers can be obtained by the fully 3-D EM simulator HFSS [40].
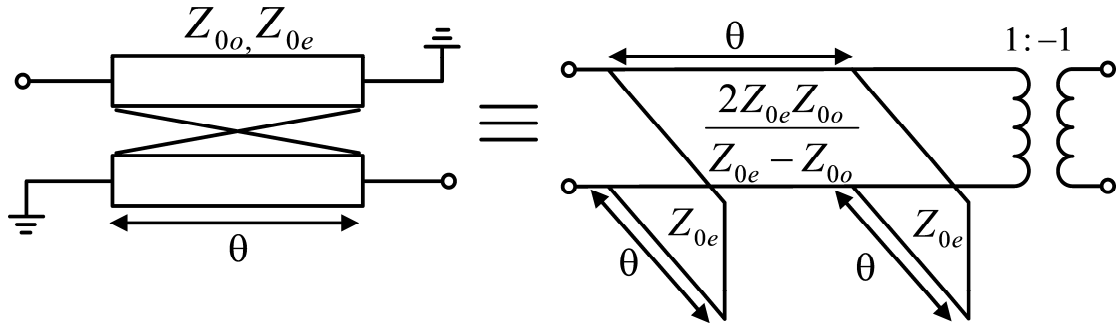
Fig. 3-9. Equivalent circuit of a short-ended coupled line.

TABLE 3-1

VIP coupler parameters extracted by HFSS (f_0=2 GHz)

Z (Ω)	H (mil)	W (mil)	ε_{re}	ε_{ro}	Z_{0e} (Ω)	Z_{0o} (Ω)	L (mil)
59.0	70	21.5	1.28	2.87	348.0	27.2	894.0
50.8	70	25.9	1.26	2.91	336.0	23.5	886.0
41.3	70	34.0	1.24	2.97	320.6	19.4	875.5
29.8	70	49.0	1.22	3.04	297.5	14.2	862.0

Four cases of VIP couplers are calculated for the prototype circuits in the next section. The physical parameters in Fig. 3-8 and the calculated electrical parameters of the VIP couplers are listed in Table 3-1 where L is the required physical length of the short-ended VIP coupler to provide 270^0 phase-shifting at the center frequency of 2GHz. Fig. 3-10 shows the simulated 15-dB equal-ripple return loss bandwidth of a 3-dB single-section hybrid ring with a short-ended coupler versus different Z_{0e}. It can be seen that the bandwidth approaches to an asymptotic value as long as Z_{0e} is higher than about 250Ω. Therefore, if the VIP coupler can have this high Z_{0e} value, a nearly ideal single-section unit can be implemented. Besides, the VIP coupler can also provide a good crossover in the proposed circuit. Because the signal going through the short-ended VIP coupler is mainly odd-mode and the field of odd-mode is mostly confined in the VIP substrate, the crossover has negligible influence on circuit performance.
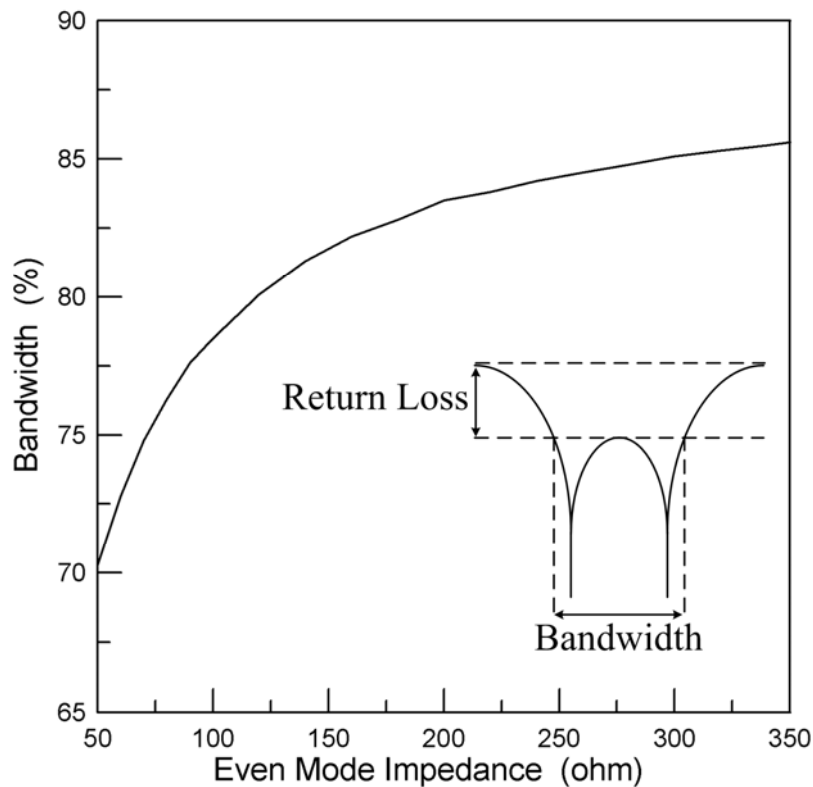
Fig. 3-10. Simulated 15-dB equal-ripple return loss bandwidth of a 3-dB single-section hybrid ring with a short-ended coupler versus different Z_{0e}.

3.3 Experimental results and discussion

As we mentioned previously, the VIP coupler is a good candidate to realize the phase inverter and the crossover on microstrip circuits. Four prototype circuits are fabricated that all of them are with a 15-dB of equal-ripple return loss. Four prototype circuits are a single-section reconfigured 3-dB hybrid ring to observe the performance of the single-section building block, a two-section 3-dB hybrid ring with the equivalent circuit shown in Fig. 3-1(c) to verify the validity of the theory derived in previous section, a two-section 20-dB hybrid ring to show the high power-division ratio of the proposed design in Fig. 3-1(c), and a two-section 3-dB hybrid ring with the equivalent circuit shown in Fig. 3-2 to depict the bandwidth extension performance.

The 3-D view of the reconfigured single-section hybrid ring is shown in Fig. 3-11 and the photograph of the reconfigured and conventional 3-dB hybrid rings is depicted in Fig. 3-12. The required VIP coupler parameters with Z=59Ω are also shown in Table 3-1. It can be seen that the reconfigured single-section hybrid ring is

compact compared to the conventional one. The measured performance, although not shown, is very close to theoretical results. This is the basic building block of next three two-section hybrids.
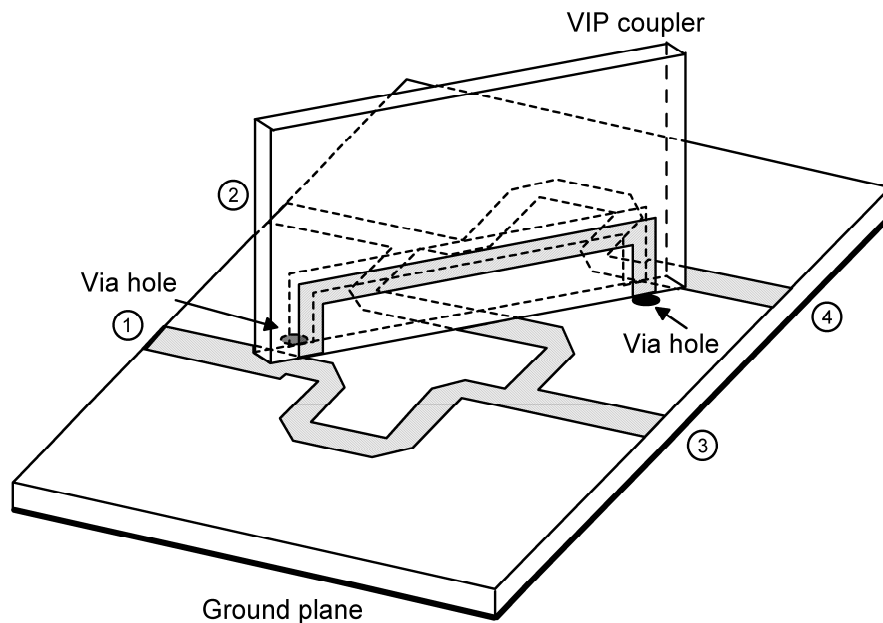
Fig. 3-11. 3-D structure of the single-section hybrid ring using the VIP coupler.

The two-section 3-dB hybrid ring with the equivalent circuit shown in Fig. 3-1(c) and a photograph shown in Fig. 3-13(a) has the line impedances of Z_1=99.60Ω and Z_2=41.26Ω. The designed passband is 1.04-2.96GHz (96% bandwidth). Fig. 3-14 shows the simulated and measured results and the measured insertion loss is approximately 0.4dB. The measured return losses are better than 10 dB from 1.06 to 3GHz for out-of-phase operation and from 1.16 to 3.04GHz for in-phase operation, respectively. The measured isolation is typically better than 20 dB from 0.5 to 3.5 GHz. The measured amplitude and phase imbalances are shown in Fig. 3-15. For out-of-phase operation, the amplitude imbalance is within 1 dB from 1.06 to 3.1GHz and the phase imbalance is within 10^0 from 1.08 to 3.5GHz. For in-phase operation, the amplitude imbalance is within 1 dB from 0.96 to 3.5GHz and the phase imbalance is within 10^0 from 0.5 to 3.5GHz. The required VIP coupler parameters with Z=41.3Ω are shown in Table 3-1.
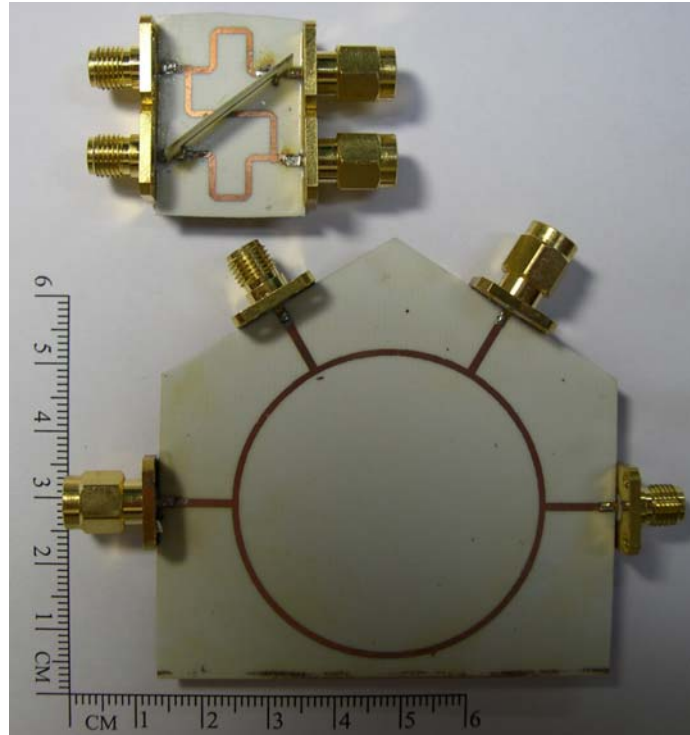
Fig. 3-12. Fabricated circuits of the conventional and reconfigured single-section hybrid rings.

The two-section 20-dB hybrid ring with the equivalent circuit shown in Fig. 3-1(c) and a photograph shown in Fig. 3-13(b) has line impedances of $Z_1=56.21\Omega$ and $Z_2=50.84\Omega$. The measured and simulated results are shown in Fig. 3-16. The designed passband is 1.144-2.856GHz (85.5% bandwidth). The measured equal-ripple return loss bandwidth is a little narrower than the simulated result. The measured isolation is better than 25 dB from 0.5 to 3.5 GHz. The measured phase performances are not shown here because they are not important for loose coupling. The required VIP coupler parameters with $Z=50.8\Omega$ are shown in Table 3-1. In contrast, a single section 20-dB hybrid ring with unit element should have $Z_1=364.1\Omega$, $Z_2=36.41\Omega$, and Z_T (impedance of a unit element) $=38.9\Omega$ which can hardly be realized by microstrip or CPW circuit. The single section 20-dB hybrid ring without unit element has higher impedance values that are more difficult to implement.

The two-section 3-dB hybrid ring with the equivalent circuit shown in Fig. 3-2 and a photograph shown in Fig. 3-13(c) has the line impedances of $Z_1=71.48\Omega$, $Z_2=29.61\Omega$, $Z_3=34.29\Omega$, and $Z_4=29.12\Omega$. The designed passband is 0.66-3.34GHz (134% bandwidth). Fig. 3-17 shows the simulated and measured results and the

33

measured insertion loss is approximately 0.6dB. The measured return losses are better than 10 dB from 0.72 to 3.38GHz for out-of-phase operation and from 0.82 to 3.36GHz for in-phase operation, respectively. The measured isolation is better than 20 dB from 1.16 to 3.5 GHz. The measured amplitude and phase imbalances are shown in Fig. 3-18. For out-of-phase operation, the amplitude imbalance is within 1 dB from 0.72 to 3.5GHz and the phase imbalance is within 10^0 from 0.9 to 3.3GHz. For in-phase operation, the amplitude imbalance is within 1 dB from 0.72 to 3.36GHz and the phase imbalance is within 10^0 from 0.76 to 3.38GHz. The required VIP coupler parameters with Z=29.8Ω are shown in Table 3-1.


(a)   (b)

(c)
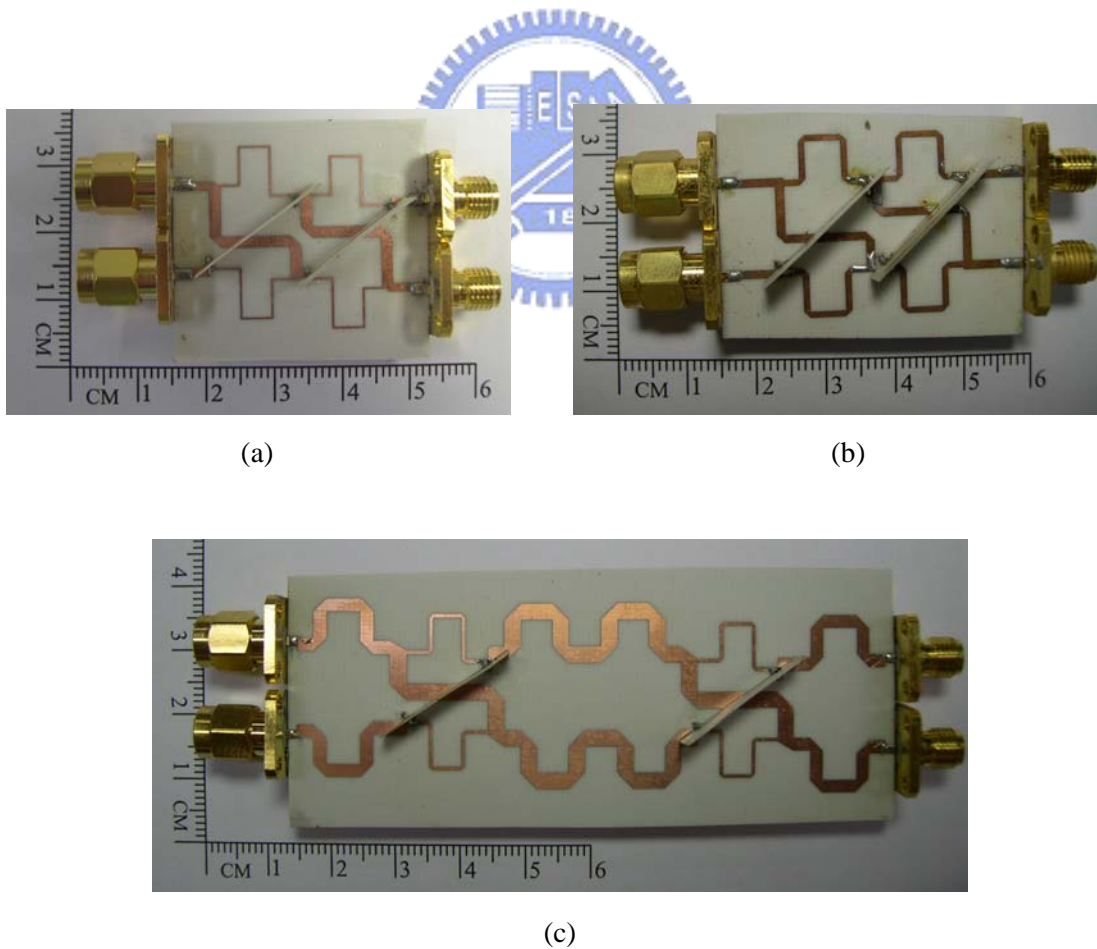
Fig. 3-13. Fabricated two-section hybrid rings (a) 3-dB hybrid ring (b) 20-dB hybrid ring (c) 3-dB hybrid ring with a unit element at each I/O port.

(a)
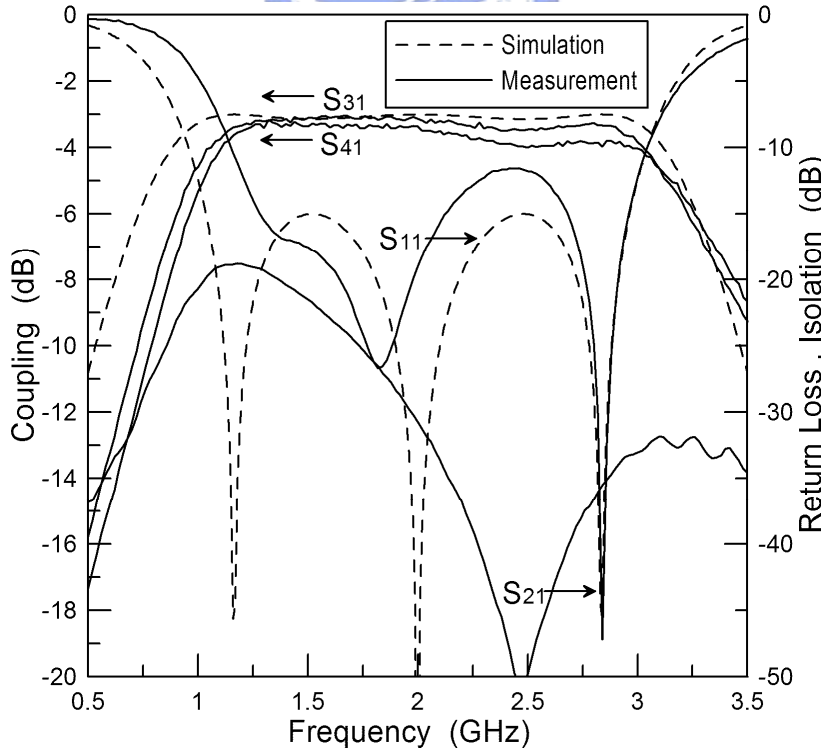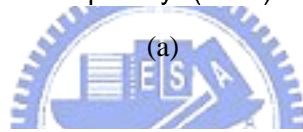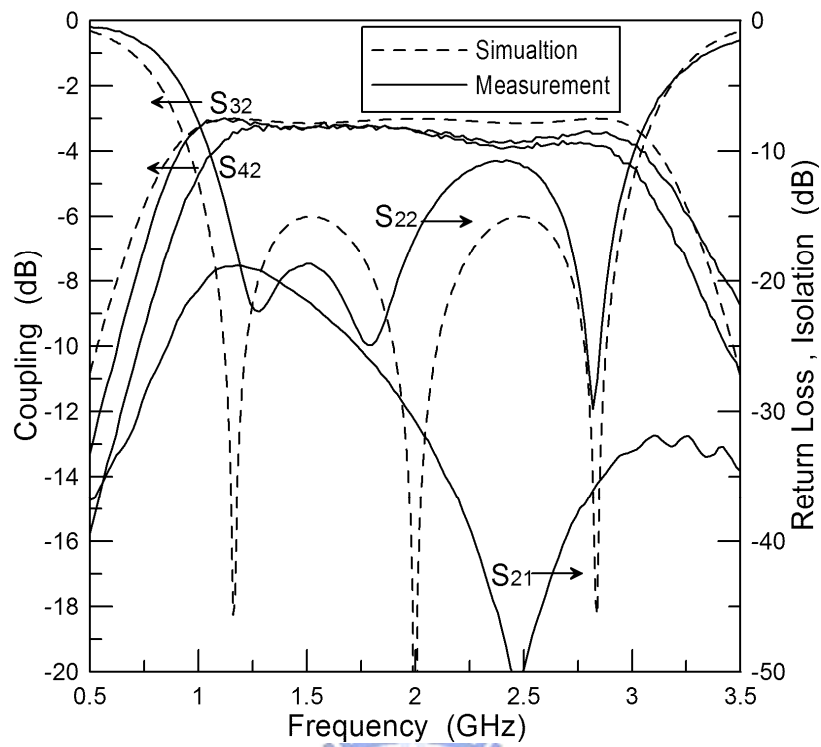
(b)

Fig. 3-14. Measured and simulated results of the 3-dB two-section hybrid ring (a) Out-of-phase operation (b) In-phase operation.
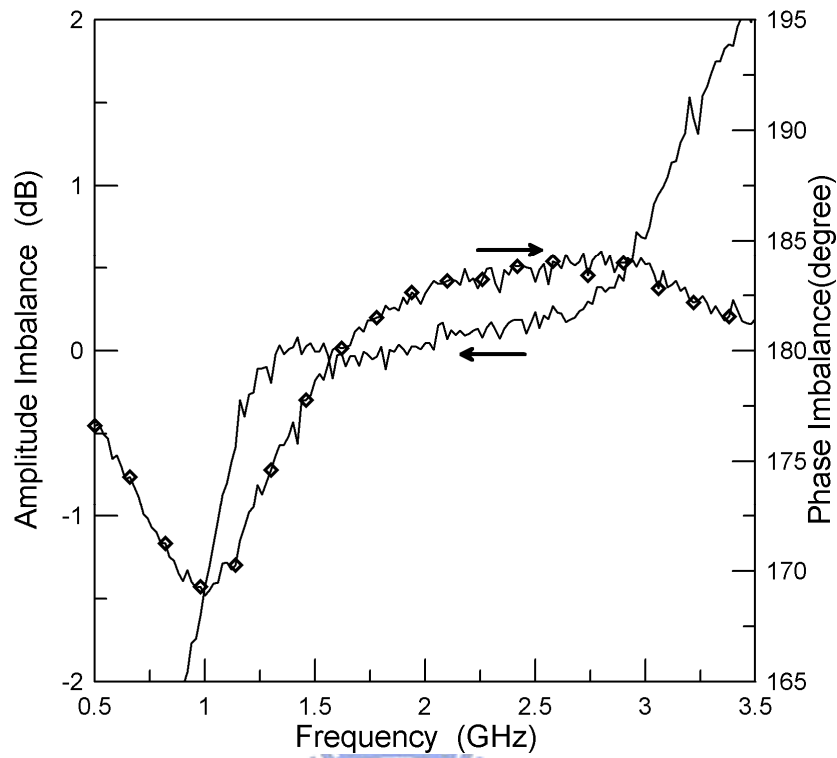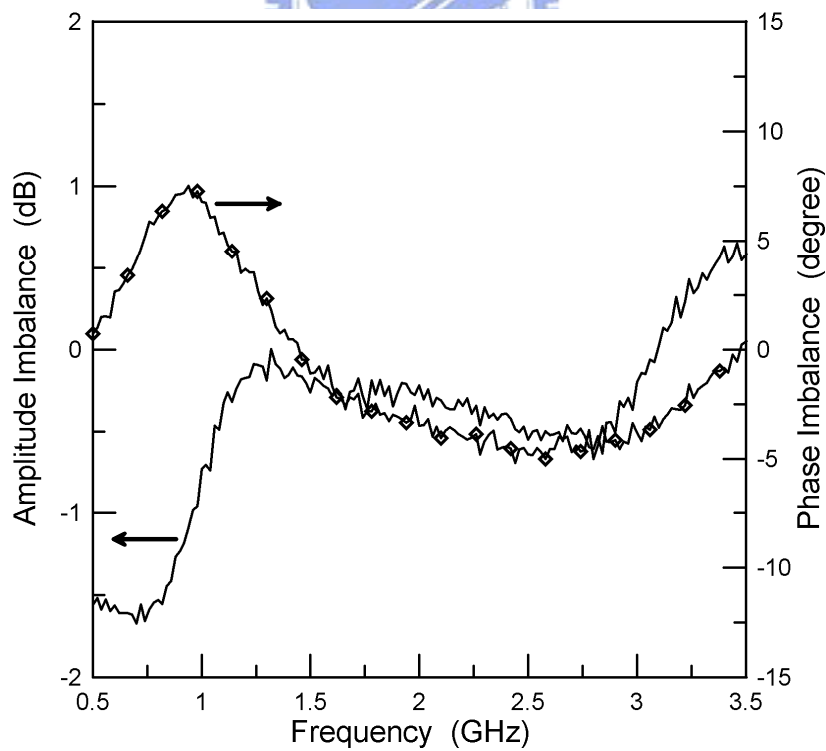
Fig. 3-15. Measured amplitude and phase imbalances of the 3-dB two-section hybrid ring (a) Out-of-phase operation (b) In-phase operation.
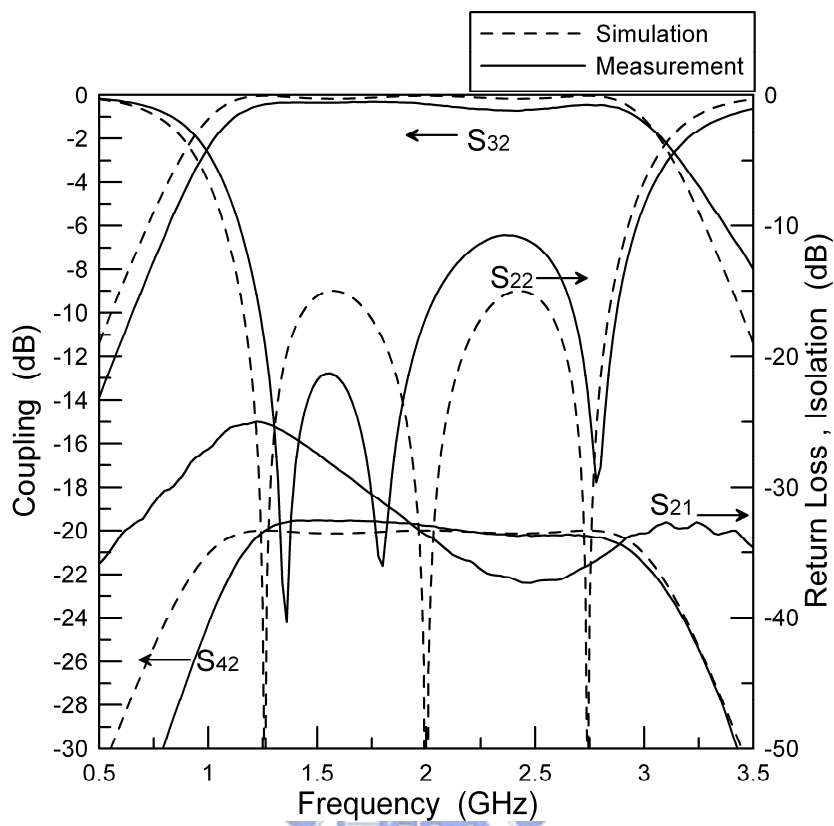
Fig. 3-16. Measured and simulated results of the 20-dB two-section hybrid ring.

(a)

37
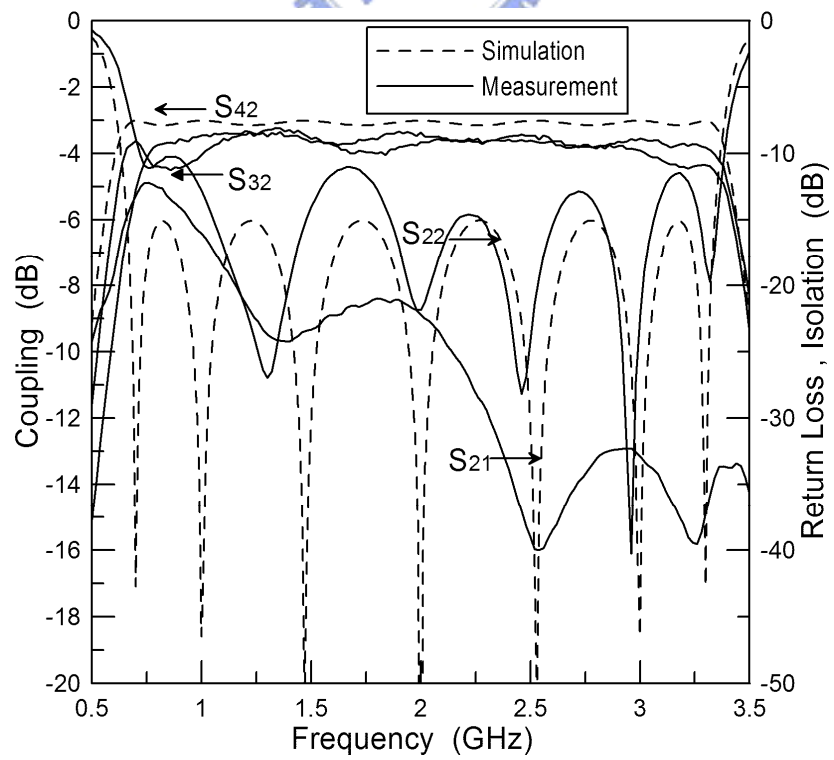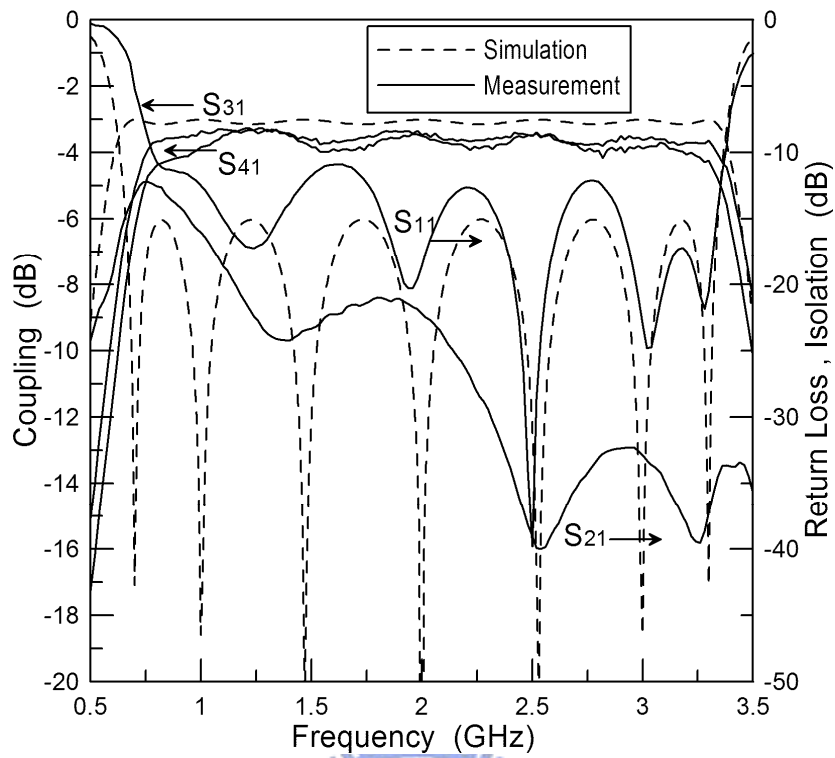
Fig. 3-17. Measured and simulated results of the 3-dB two-section hybrid ring with a unit element at each I/O port (a) Out-of-phase operation (b) In-phase operation.
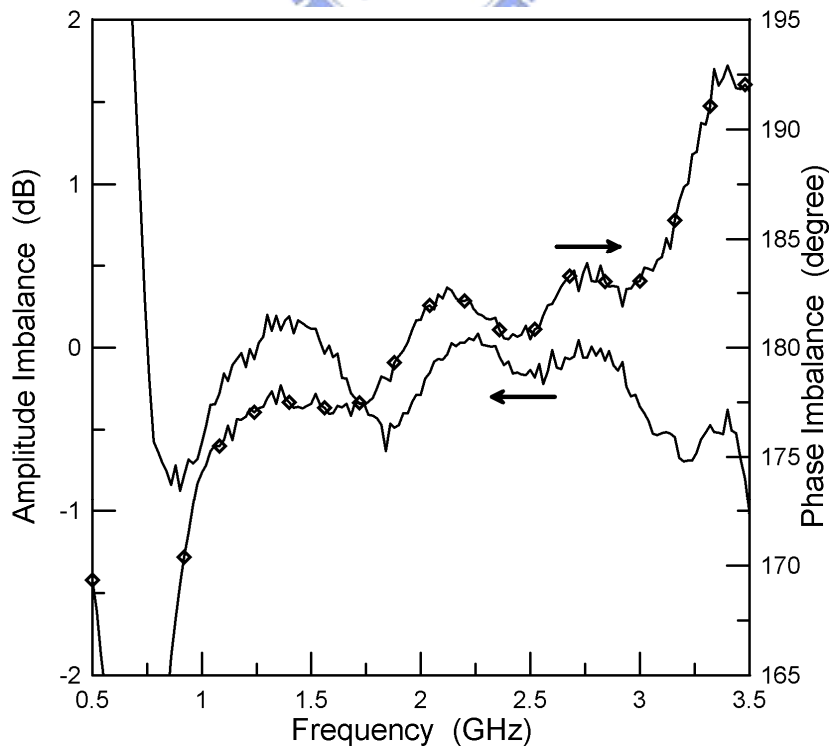
(a)
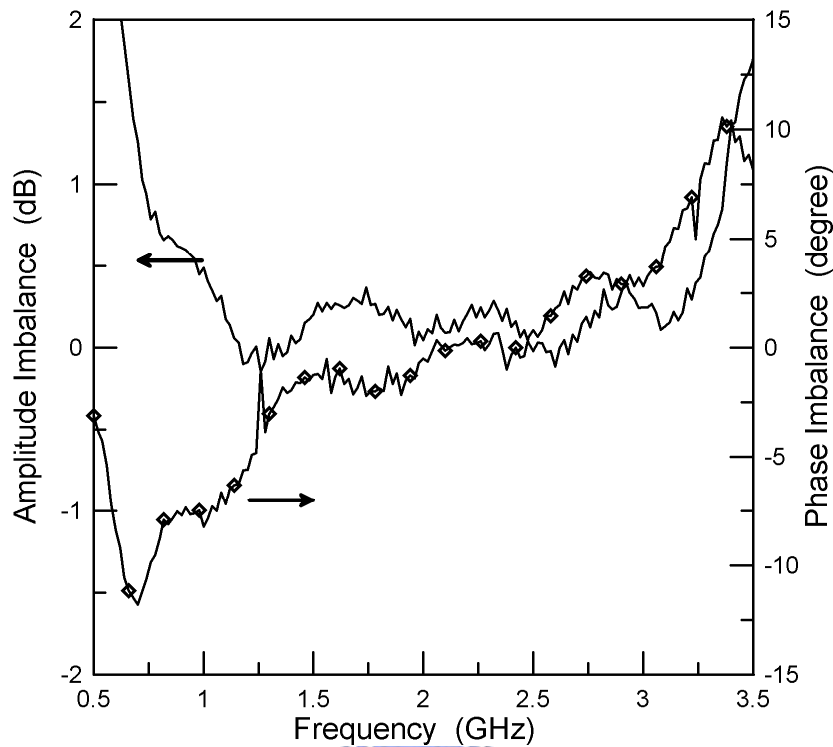
(b)

Fig. 3-18. Measured amplitude and phase imbalances of the 3-dB two-section hybrid ring with a unit element at each I/O port (a) Out-of-phase operation (b) In-phase operation.

The above measured results indicate the bandwidth of the two-section cascadable hybrid rings using the VIP coupler is a little narrower than that using an ideal phase inverter, especially for in-phase operation. It should be point out that the simulated performances in Figs. 3-14, 3-16, and 3-17 are based on an ideal single-section unit. The bandwidth shrinkage is due to the fact that the infinity value of Z_{0e} is impractical to be fabricated. In previous section, we have shown that if the Z_{0e} higher than 250 Ω, the performance of a single-section unit approaches to an ideal hybrid ring. Nevertheless, the characteristics of a single-section unit equal to those of an ideal hybrid ring only when Z_{0e} is infinity. Therefore, the bandwidth is shrunk due to finite Z_{0e} especially in the cascaded case. In addition, the junction effect (especially junctions at microstrip and VIP coupler) and circuit fabricating imperfections degrade the bandwidth further.

Chapter 4

Wideband Bandpass Filters with Wide Upper Stopband Using Stepped-Impedance Rat-Race Hybrid Couplers

In this chapter, we propose the wideband bandpass filter using two 180^0 hybrid ring couplers. Then, by adding one pair of quarter-wave transmission lines between two hybrid ring couplers, this filter can exhibit wider bandwidth. Finally, by employing two pairs of quarter-wave transmission lines, the two rat-race hybrid couplers can be connected without crossover. In addition, compared to the basic structure, using two pairs of quarter-wave transmission lines for connections can increase the order and bandwidth of the filter. Therefore, we use two rat-race hybrid couplers and two pairs of quarter-wave transmission lines with a stepped-impedance structure to design a wideband bandpass filter. The filter with the stepped-impedance structure acquires not only size reduction, but also better upper stopband clearance.
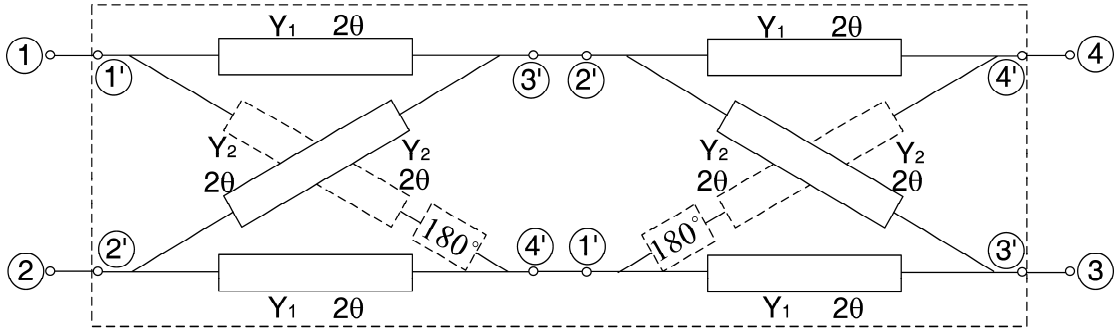
Fig. 4-1. Schematic of the proposed wideband bandpass filter using two 180^0 hybrid ring couplers.

4.1 Bandpass filter by cascading two 180^0 hybrid couplers

Fig. 4-1 shows the schematic of the proposed wideband bandpass filter using two 180^0 hybrid ring coupler. It should be noted that the schematic shown in Fig. 4-1 is different from that shown in Fig. 3-1(c) at the connections of ports. Based on the analysis method mentioned in section 3.1, the S-parameters of the proposed wideband bandpass filter shown in Fig. 4-1 can be expressed as

$$S_{11} = S_{22} = S_{33} = S_{44}$$
$$= \frac{2[B^2(A+2C+D)+B(2+A^2-2C^2+D^2)]-2C(2+A^2+AC+CD+D^2)}{(A+B+C+D)(A+2B+D)(A+2C+D)}$$

$$S_{21} = S_{43} = 0$$

$$S_{31} = S_{42} = 0$$

$$S_{41} = S_{32} = \frac{4+(A-D)^2}{(A+2B+D)(A+2C+D)}. \tag{4-1}$$

All of the power excited at port 1 will be delivered to port 4 and no power reaches port 3 and port 2. Also, we can obtain

$$\frac{(Y_1+Y_2)(1-Y_1^2-Y_2^2)}{Y_1^2+Y_2^2} - m(\frac{2}{x_c}+\frac{\sqrt{1-x_c^2}}{x_c}) = 0. \tag{4-2}$$

$$\frac{(Y_1+Y_2)(-1+Y_1^2+2Y_1Y_2+Y_2^2)}{Y_1^2+Y_2^2} + m(\frac{2}{x_c^3}+\frac{2\sqrt{1-x_c^2}}{x_c^3}) = 0. \tag{4-3}$$

The relationship between m and return loss (RL) is

$$RL = 10\log(1 + 1/m^2) \; dB. \tag{4-4}$$

Here, we assume that the relationship between Y_1 and Y_2 is

$$\frac{Y_1}{Y_2} = r. \tag{4-5}$$

Equations (4-2)-(4-5) can be used to design the wideband bandpass filter with a given return loss and relationship r between Y_1 and Y_2. Fig. 4-2 and Fig. 4-3 show the plots of Z_1 and Z_2 versus bandwidth for 15-dB and 20-dB equal-ripple return loss, respectively. It can be found that the higher Z_2 to Z_1 impedance ratio is, the broader the bandwidth of the filter can achieve.
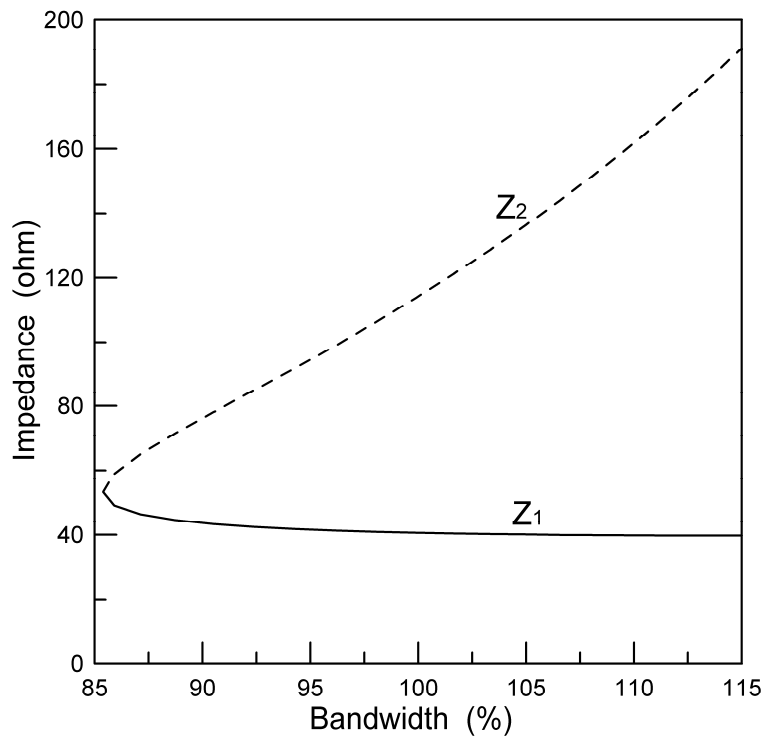
Fig. 4-2. Characteristic impedances Z_1 and Z_2 versus bandwidth for the wideband bandpass filter with 15-dB equal-ripple return loss.
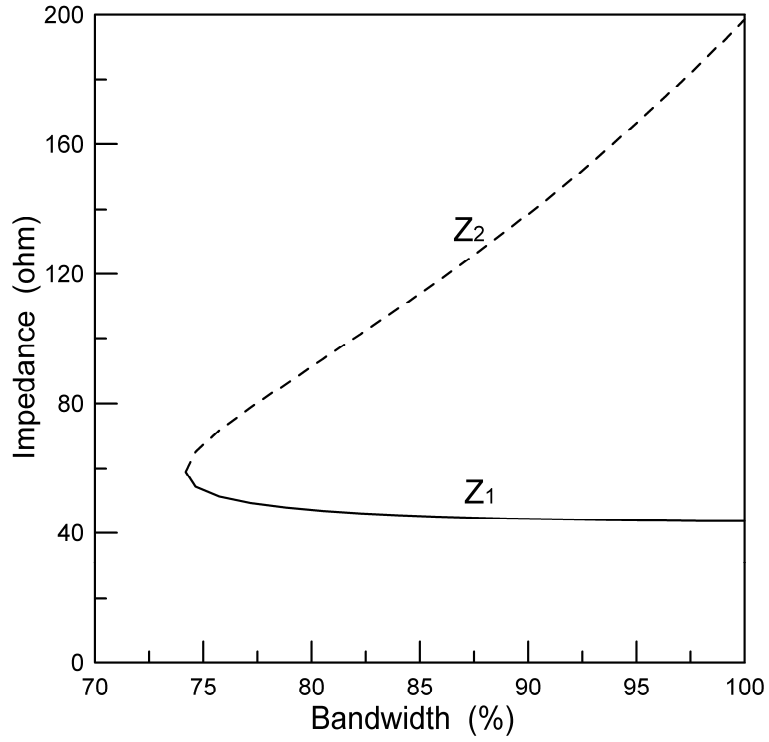
Fig. 4-3. Characteristic impedances Z_1 and Z_2 versus bandwidth for the wideband bandpass filter with 20-dB equal-ripple return loss.
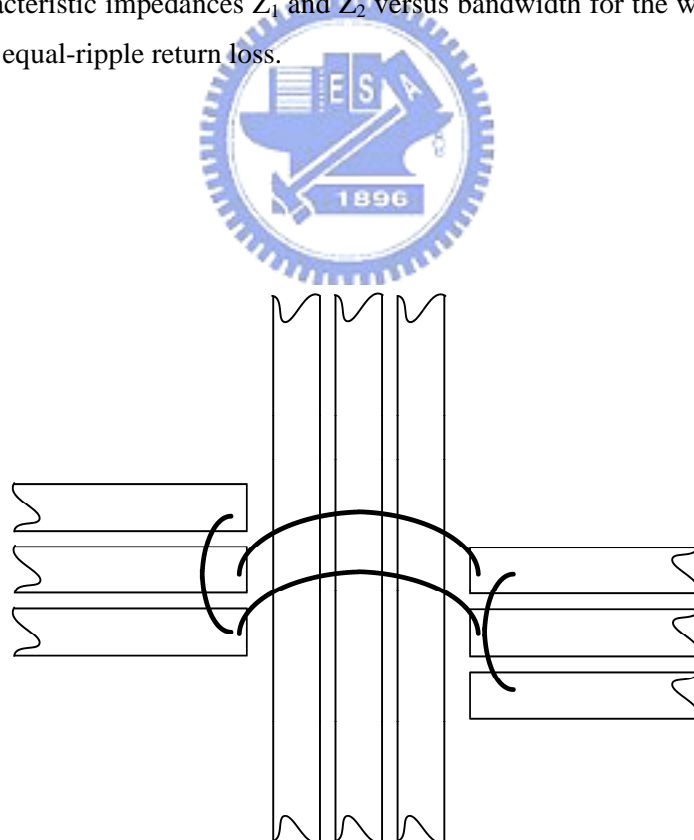
Fig. 4-4. Circuit configuration of the realized phase inverter and crossover.

The wideband phase inverter formed by a FGCPW (finite ground-plane-width CPW) twisted line can be adopted for the realization of this proposed filter. In the mean time, there are two crossovers as shown in Fig. 4-1. Fortunately, phase inverters and crossovers can be combined. The circuit configuration of the realized phase inverter and crossover using FGCPW is shown in Fig. 4-4. This wideband bandpass filter is fabricated on an Al_2O_3 alumina substrate with 15-mil thickness and a dielectric constant of 9.8. The wideband bandpass filter with 15-dB return loss has the line impedance of $Z_1=Z_2=53.31\Omega$ which corresponds to a passband of 1.15-2.85GHz (85% bandwidth). Fig. 4-5 shows the photograph of the proposed filter where port 1 and port 4 are terminated with 50-Ω resistors. Here, the port 2 is input port and port 3 is output port as depicted in Fig 4-1. It should be note that port 1 and port 4 can also be open-circuit or short-circuit because of good isolations in port 1 and port 4. Fig. 4-6 shows the simulated and measured results. The measured passband insertion loss is approximately 1.2dB. The measured results match very well with the simulated results.
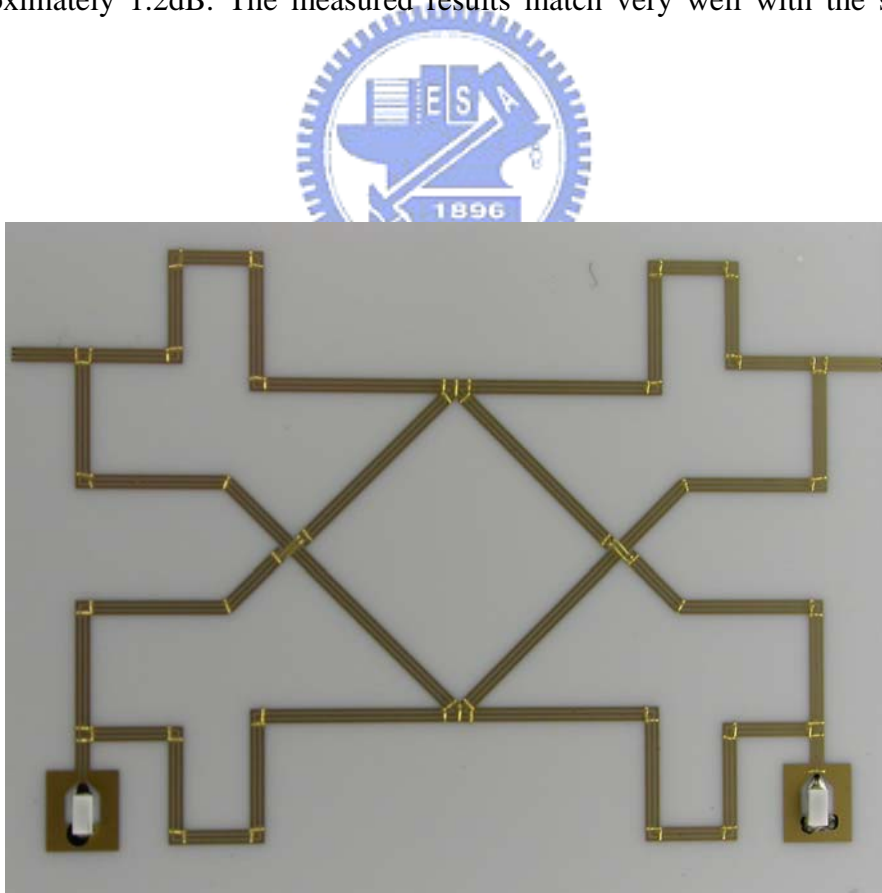
Fig. 4-5. Photograph of the fabricated filter.
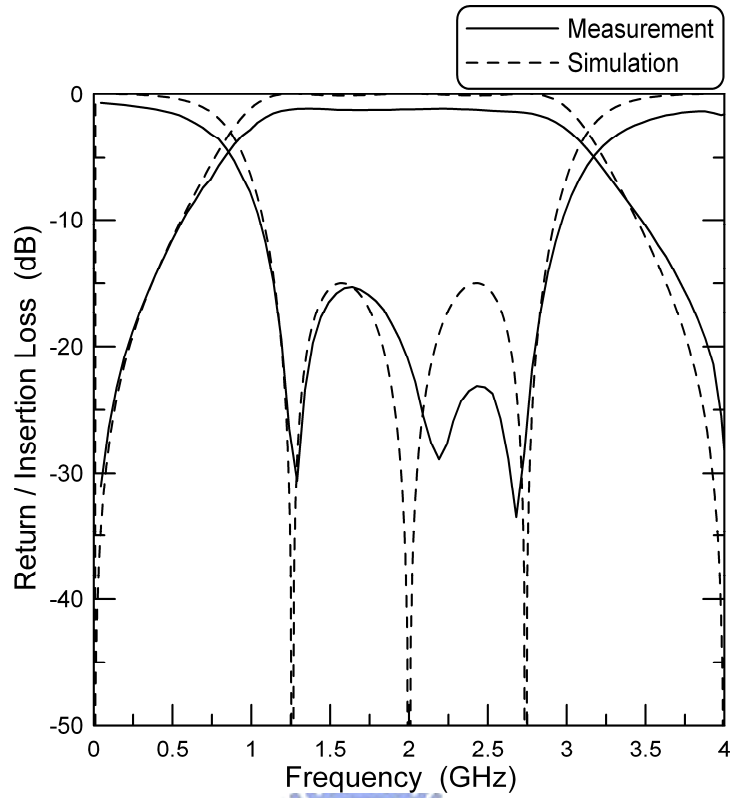
Fig. 4-6. Measured and simulated results of the wideband bandpass filter.

4.2 Bandpass filter by cascading two stepped-impedance 180^0 hybrid couplers with one unit element

(a)

(b)
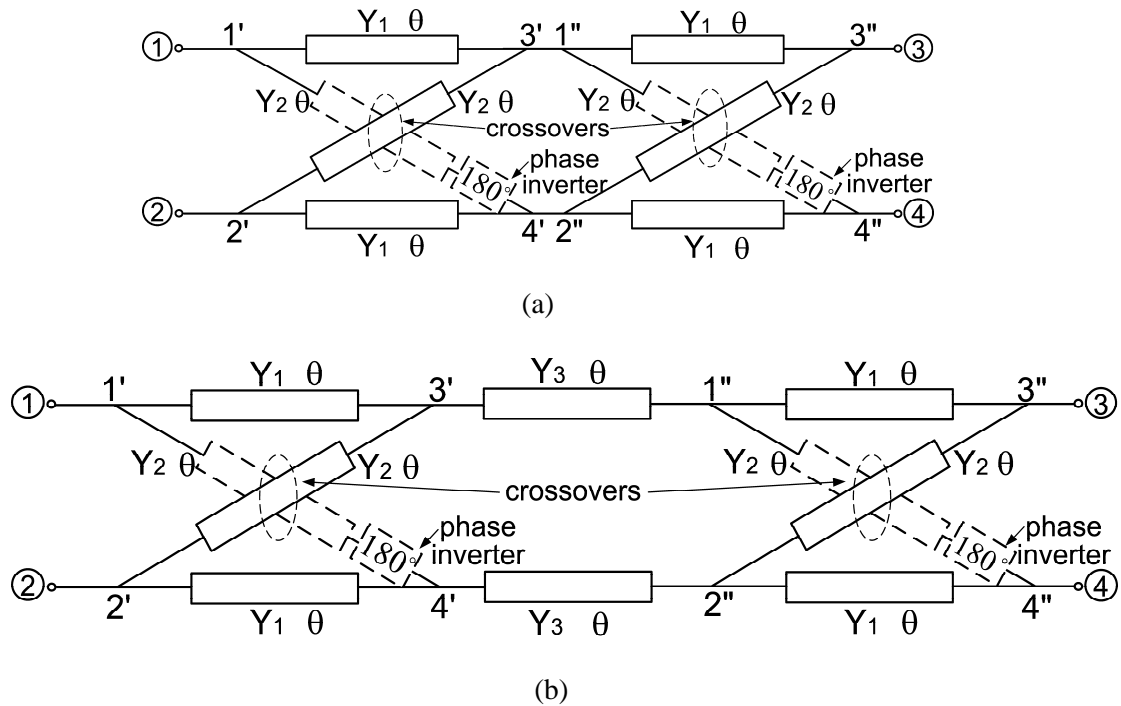
Fig. 4-7. Schematics of the proposed wideband filters (a) Basic structure (b) Modified structure .

Although the bandpass filter shown in Fig. 4-1 exhibits wide bandwidth, it still has the spurious problem. Now, consider the two-section hybrid ring shown in Fig. 4-7(a) and its S-parameters at the center frequency are

$$S_{11} = S_{22} = 0$$
$$S_{21} = S_{43} = 0$$
$$S_{31} = S_{42} = -(Y_1^2 - Y_2^2)/Y_1^2 + Y_2^2$$
$$S_{41} = -S_{32} = 2Y_1Y_2/(Y_1^2 + Y_2^2). \tag{4-6}$$

When $Y_1 = Y_2$, the signal excited at port 1 is equally divided between 3' and 4' and no power reaches 2'. The signal arriving at 3' and 4' are out of phase. Then, the signal at 3' is equally divided between 3'' and 4'' and the signal arriving at 3'' and 4'' are out of phase. The signal at 4' is equally divided between 3'' and 4'' and the signal arriving at 3'' and 4'' are in phase. Therefore, all of the power excited at port 1 will be delivered to port 4 and no power reaches port 3 and port 2 (corresponding to a 0-dB coupler). This means that a bandpass response can be obtained by cascading two 3-dB 180° hybrid rings.
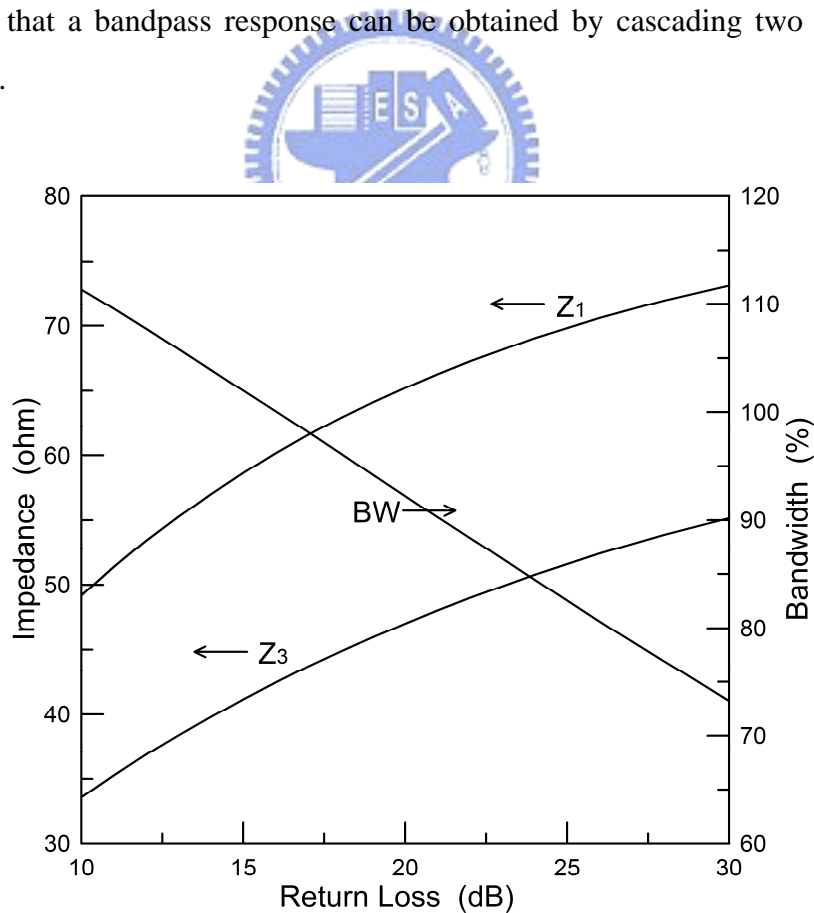
Fig. 4-8. Characteristic impedances Z_1, Z_3, and bandwidth versus return loss for the equal-ripple response bandpass filter shown in Fig. 4-7(b).
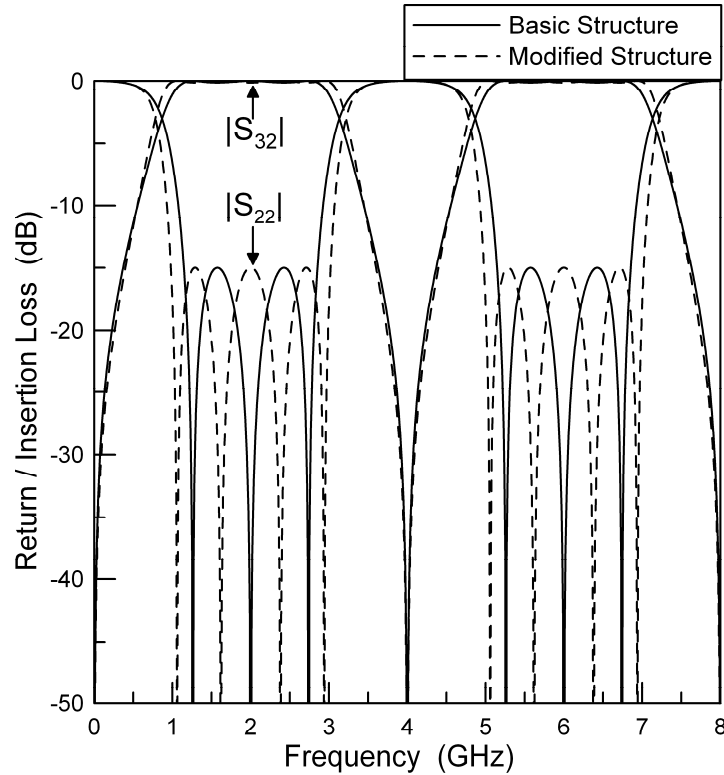
Fig. 4-9. Simulated results of the proposed wideband filter (a) Basic structure (b) Modified structure.

Here, to increase the order and the bandwidth of the proposed filter, a 90^0 transmission line of impedance Z_3 can be added between two 180° hybrids as shown in Fig.4-7(b). With the design method described in section 3.1, the bandwidth of this filter corresponding to specific return losses can be obtained. Fig. 4-8 shows the plot of characteristic impedances of Z_1, Z_3, and bandwidth versus return loss for the bandpass filter shown in Fig. 4-7(b).

The simulated results of the filters in Fig. 4-7(a) and 4-7(b) with 15-dB return loss are depicted in Fig. 4-9 that they correspond to third ($Z_1=Z_2=53.31\Omega$) and fourth ($Z_1=Z_2=58.65\Omega$ and $Z_3=41.16\Omega$) order filter respectively. Although wide passband can be easily achieved, the first spurious passband at $3f_0$ results in poor upper stopband performance. In chapter 2, the frequency of the first spurious response of the 180° hybrid ring can be moved using the stepped-impedance structure by adjusting its structural parameters. Thus, by applying the stepped-impedance structure to Fig. 4-7(b), a wideband filter with broad upper stopband characteristics can be obtained. The design procedures are summarized as follow:

Step 1) Specify the required return loss and obtain the corresponding circuit parameters in Fig. 4-7(b). This can be easily obtained from Fig. 4-8. (15dB-

47

return loss, $Z_1=Z_2=58.65\Omega$ and $Z_3=41.16\Omega$ in this design)

Step 2) Employ the stepped-impedance structure to each line section in Fig. 4-7(b). For a given θ_H and θ_L, parameters (Z_H and Z_L) of the stepped-impedance circuit equivalent to a quarter-wave transmission line of the specific impedance can be calculated by using (2-3)-(2-5). These are the initial parameters of the bandpass filter.

Step 3) Fine-tune the circuit parameters to optimize the circuit performance.

The optimized circuit parameters are shown in Table 4.1.

Following the above-described design steps, the circuit parameters of the proposed bandpass filter can be obtained. However, the realization of a wideband 180^0 phase inverter on microstrip circuits would be a problem. This can be solved by using a $\lambda/4$ short-ended coupled line with the VIP structure. Therefore, the ideal 180^0 phase inverter and crossovers, shown in Fig. 4-7, are implemented by a $\lambda/4$ short-ended coupled line with the VIP structure. Then, we employ stepped-impedance structure to the $\lambda/4$ short-ended VIP coupler. To simplify this design, the short-ended stepped-impedance VIP coupler is approximately equivalent to a balanced stepped-impedance transmission line with 180° of twist (physically 180° of twist equivalent to an ideal 180° phase inverter). This equivalence is valid as long as the even- to odd-mode impedance ratio is large. The characteristic impedance of each balanced line section approximately equals to $2Z_{0e}Z_{0o}/(Z_{0e}-Z_{0o})$. Its physical length can be determined by the effective odd-mode dielectric constant because the signal going through it is mainly odd-mode. Fine tuning the length of each VIP line section to fit the insertion phase of other three step impedance lines at the center frequency may be required. Both the main circuit and the VIP couplers are implemented on a RO4003 substrate with thickness (h_v and h_s) of 20-mil and dielectric constant (ε_{r1} and ε_{r2}) of 3.38. The filter is designed to operate at the center frequency of 2 GHz.

Based on the above-described method, the characteristic impedances and effective dielectric constants for even- and odd-modes of the VIP coupler can be obtained by the 3-D EM simulator (Ansoft HFSS) as given in Table 4-2. Fig. 4-10 indicates the geometry of the fabricated filter. The 3-D structure and photograph of the proposed wideband filter is shown in Fig.4-11 where port 2 and port 3 are the input and output port, respectively. Both port 1 and port 4 are isolated ports and are terminated with a

50-Ω load.

TABLE 4-1

Parameters of the stepped-impedance bandpass filter

	Z_H (Ω)	Z_L (Ω)	θ_H (Degree)	θ_L (Degree)
λ/4, Z=58.65Ω	97	29	30	19.5
λ/4, Z=41.16Ω	84	23	22.3	20

TABLE 4-2

Computed results by HFSS (f_0=2 GHz)

Z (Ω)	H (mil)	W (mil)	ε_{re}	ε_{ro}	Z_{0e} (Ω)	Z_{0o} (Ω)
59.0	70	21.5	1.28	2.87	348.0	27.2
50.8	70	25.9	1.26	2.91	336.0	23.5
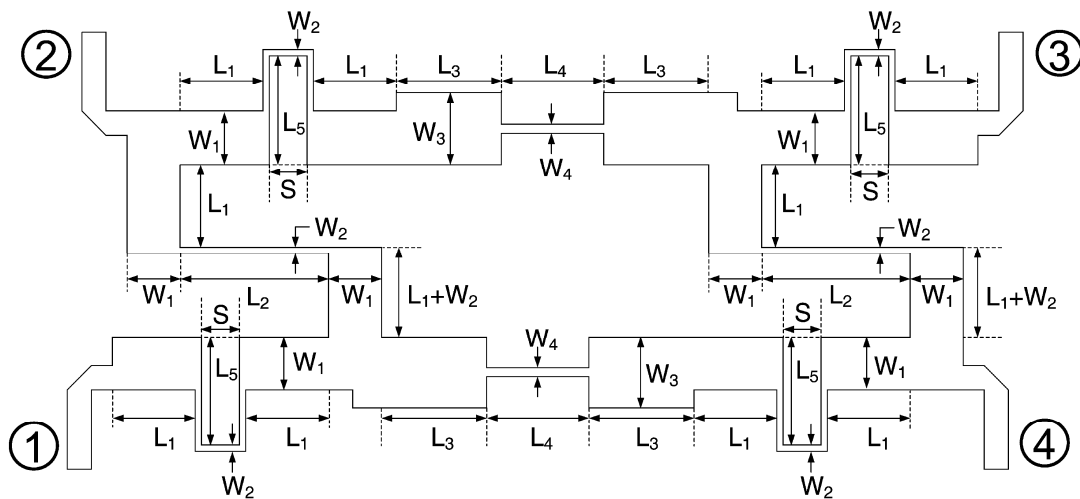
(a)
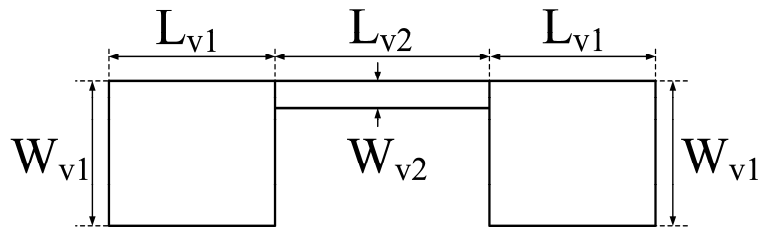
(b)

Fig. 4-10. Geometry of the fabricated filter (a) Main circuit section. W_1=101 mil, W_2=12 mil, W_3=135 mil, W_4=17 mil, S=82 mil, L_1=158 mil, L_2=283 mil, L_3=200 mil, L_4=195 mil, L_5=201 mil (b) VIP stepped-impedance coupler. W_{v1}=133 mil, W_{v2}=29 mil, L_{v1}=184 mil, L_{v2}=296 mil.

Fig. 4-12 shows the simulated and measured results of the proposed filter and the measured insertion loss is approximately 0.4dB. Note that the simulated results of the proposed filter are simulated with the computed parameters in Table 4-2 by the circuit simulator (AWR Microwave Office). The measured 10-dB return loss bandwidth is from 0.95 to 2.8 GHz (92.5%). The stopband rejection is better than -20dB from 3.3 to 6.8 GHz. The measured bandwidth is a little narrower than the simulated responses and the experimental stopband rejection is a little worse than the simulated results. This may be caused by the junction effect (especially junctions at microstrip and VIP coupler) and circuit fabricating imperfections.
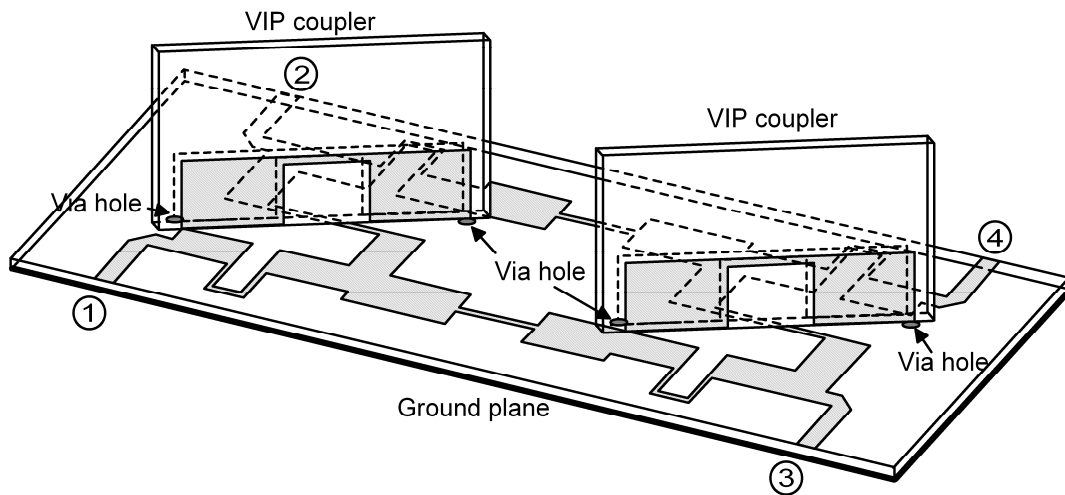
(a)
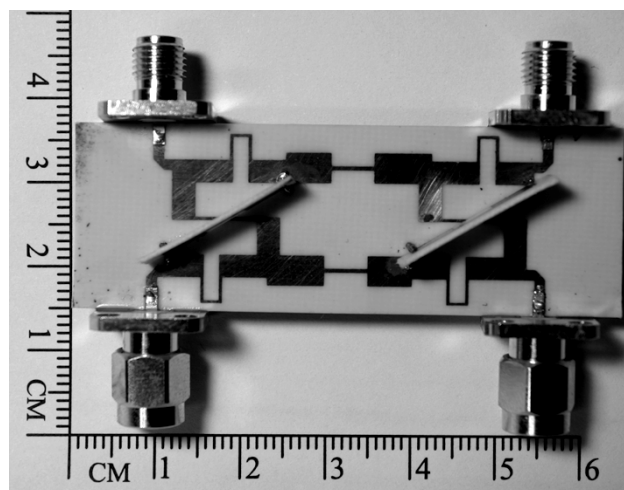
(b)

Fig. 4-11. (a) 3-D structure of the proposed wideband filter with the stepped-impedance structure (b)Photograph of the fabricated filter
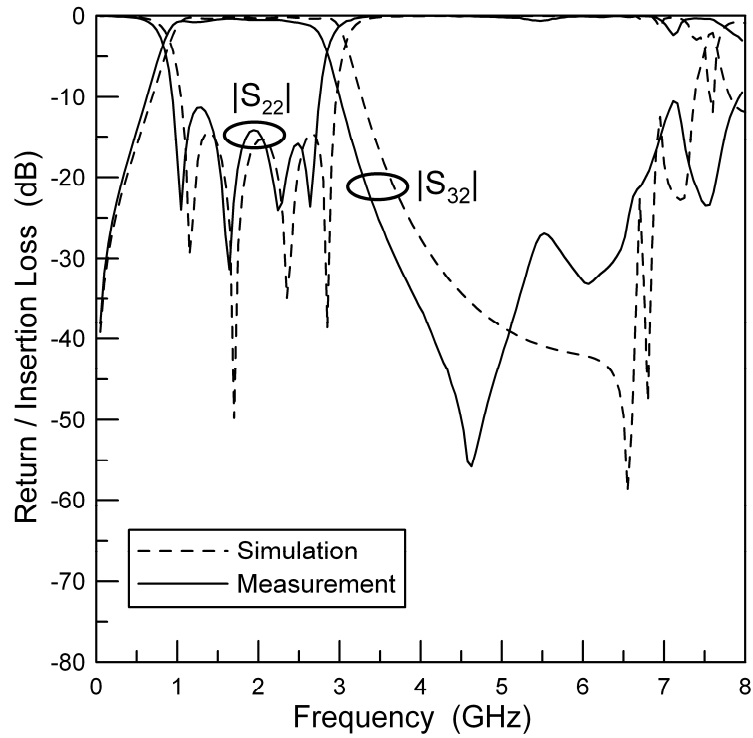
Fig. 4-12. Measured and simulated results of the proposed wideband filter with the stepped-impedance structure.

4-3 Bandpass filter by cascading two stepped-impedance 180^0 hybrid couplers with two unit elements

(a)

(b)
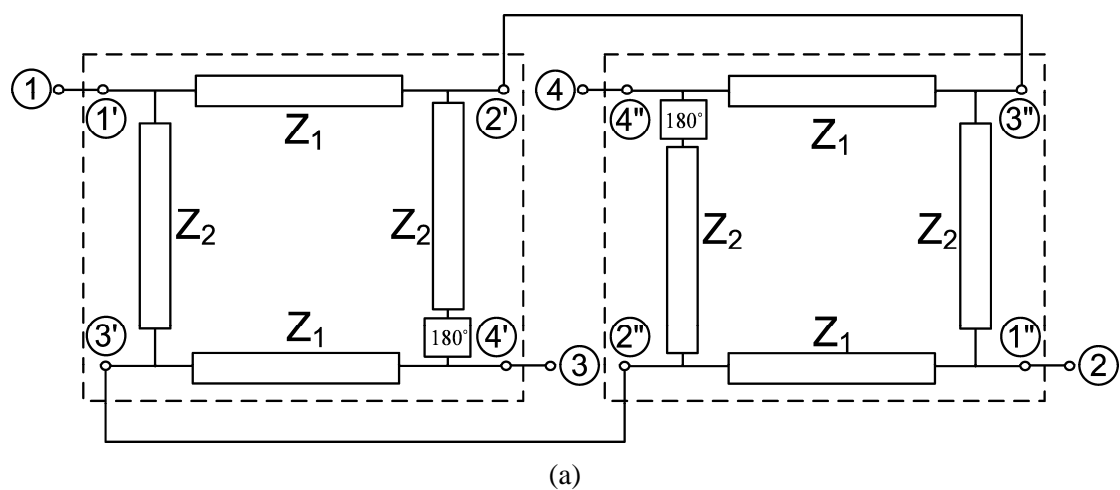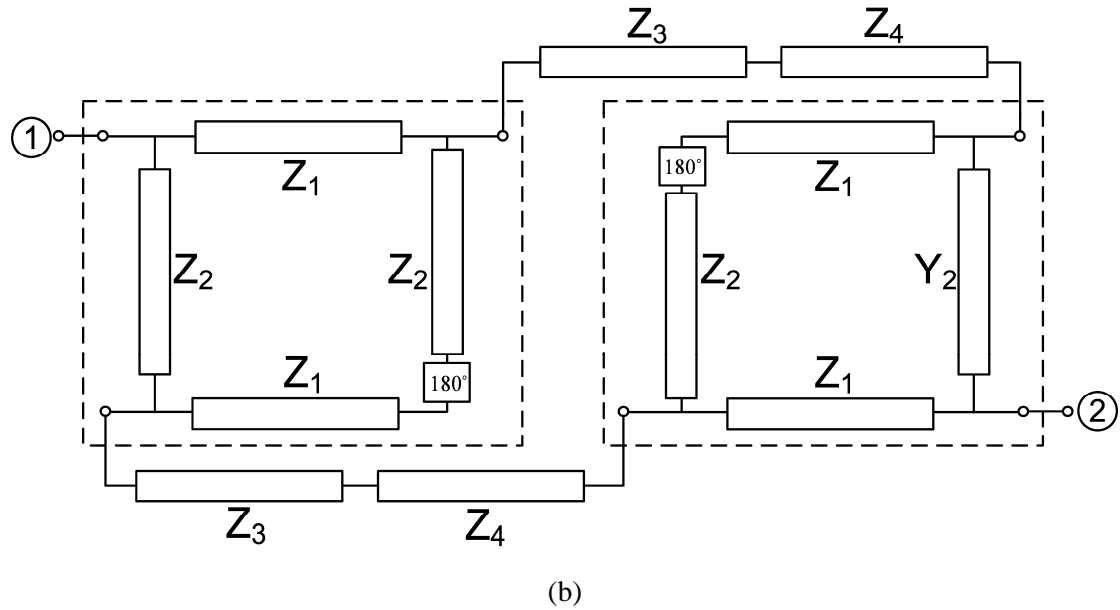
Fig. 4-13. Schematics of the proposed wideband bandpass filters with no crossover (a) Basic structure (b) Modified structure.

In the previous sections, crossovers are required to realize these bandpass filter. However, these crossovers will cause the serious parasitic problem at higher operating frequencies. Now, consider the schematic shown in Fig. 4-13(a). If the transmission line is long enough (larger than one quarter wavelength), two hybrid rings can be connected without crossover. Therefore, two hybrid rings are cascaded with two unit elements as shown in Fig. 4-13(b). Fig. 4-14 shows characteristic impedances Z_1, Z_3, and bandwidth versus return loss for the equal-ripple response bandpass filter shown in Fig. 4-13(b) with $Z_1=Z_2$ and $Z_3=Z_4$.

Following the design steps mentioned in the section 4-2, this type of the wideband bandpass filter with stepped-impedance structure can be easily designed. By increase the high/low impedance ratio of the stepped-impedance structure, the filter exhibits not only the higher first spurious passband but also smaller size. The optimized circuit parameters are listed in table 4-3. Extremely high impedance and low impedance can be realized using CPS and interdigital CPS. Besides, the wideband phase inverter can be readily implemented by using hybrid CPS/interdigital CPS structure, as mentioned in chapter 2. Therefore, hybrid CPS/interdigital CPS structure is one of the most suitable structures to implement this proposed bandpass filter.
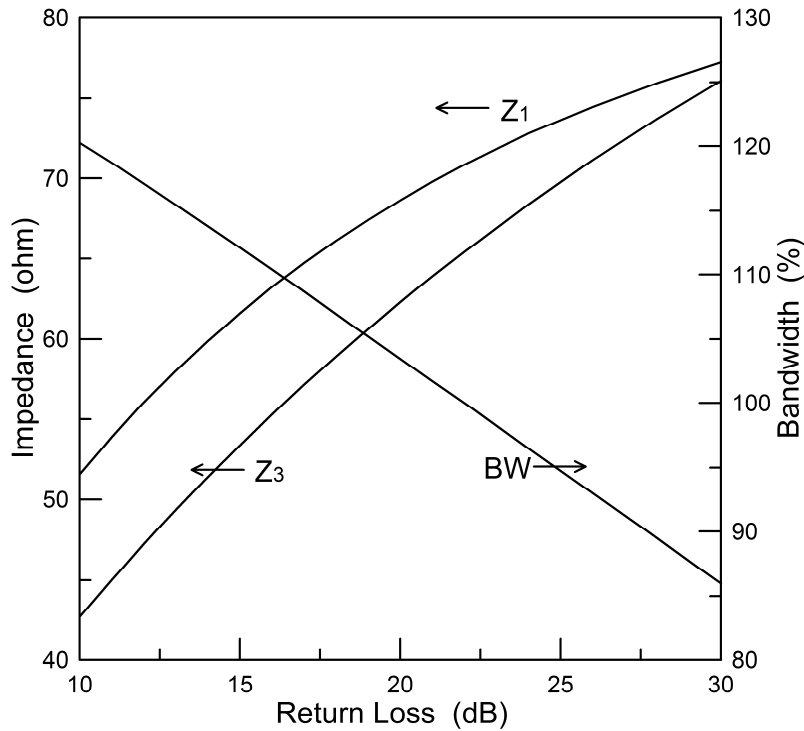
Fig. 4-14. Characteristic impedances Z_1, Z_3, and bandwidth versus return loss for the equal-ripple response bandpass filter shown in Fig. 4-13(b).

This wideband bandpass filter is fabricated on an Al_2O_3 alumina substrate with 15-mil thickness (h) and a dielectric constant (ε_r) of 9.8. This filter is designed to operate at the center frequency of 2 GHz. Using the CPS design curves provided in section 2.3, the CPS parameters can be obtained as shown in Table 4-4. The layout of the proposed wideband bandpass filter is shown in Fig. 4-15. Fig. 4-16 shows layouts of discontinuities for the proposed wideband bandpass filter. The simulated results of the proposed filter are simulated with the computed parameters in Table 4-3 by using the circuit simulator as shown in Fig. 4-17. It is should be noted that the bandwidth of the stepped-impedance bandpass filter is a little narrower than that of the quarter-wavelength structure. Fig. 4-17 also shows the simulated results of the proposed filter with discontinuity effects. It can be observed from Fig. 4-17 that the discontinuity junctions whose parasitic effects alter the frequencies of harmonics. The EM simulated results and measured results of the proposed filter are shown in Fig. 4-18. The measured insertion loss is approximately 1.2dB. The measured return loss is better than 10-dB is from about 1 to 3 GHz (100%). The stopband rejection is better than -30dB up to 17.7 GHz. In Fig.4-18, the simulated first spurious passband is

around 8.3GHz. However, due to CPS losses the spike-like spurious responses around these frequencies are not found in the measurement. Fig. 4-19 shows a photograph of the fabricated bandpass filter and the overall size is 950 mil × 642 mil.

TABLE 4-3

Parameters of the stepped-impedance bandpass filter

	Z_H (Ω)	Z_L (Ω)	θ_H (Degree)	θ_L (Degree)
λ/4, Z=61.40Ω	184	22	17.4	14.8
λ/4, Z=53.23Ω	184	22	15.4	16.8

TABLE 4-4

CPS and interdigital CPS parameters of the stepped-impedance bandpass filter

	Line width W (mil)	Gap width S (mil)	Z (Ω)
Interdigital CPS (N=3)	4	1.6	22
CPS	4	24	184
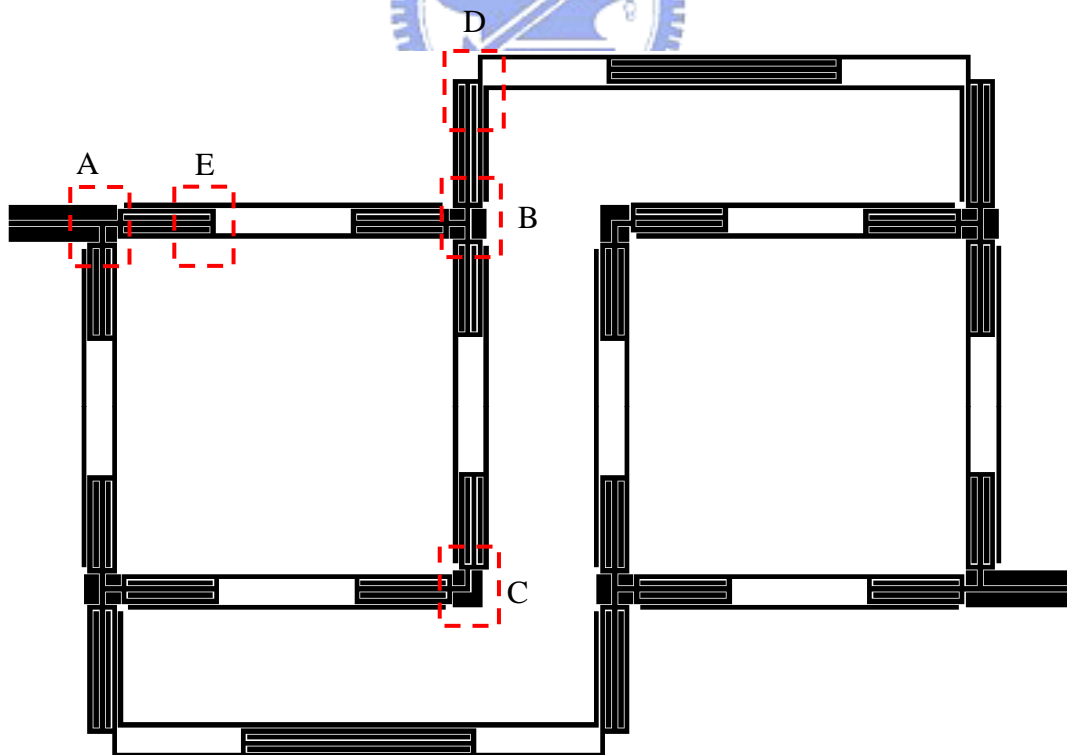
Fig. 4-15. Layout of the fabricated stepped-impedance wideband bandpass filter.

(a)

(b)   (c)

(d)   (e)

Fig. 4-16. Layouts of discontinuities (a) Discontinuity A (b) Discontinuity B (c) Discontinuity C (d) Discontinuity D (e) Discontinuity E.
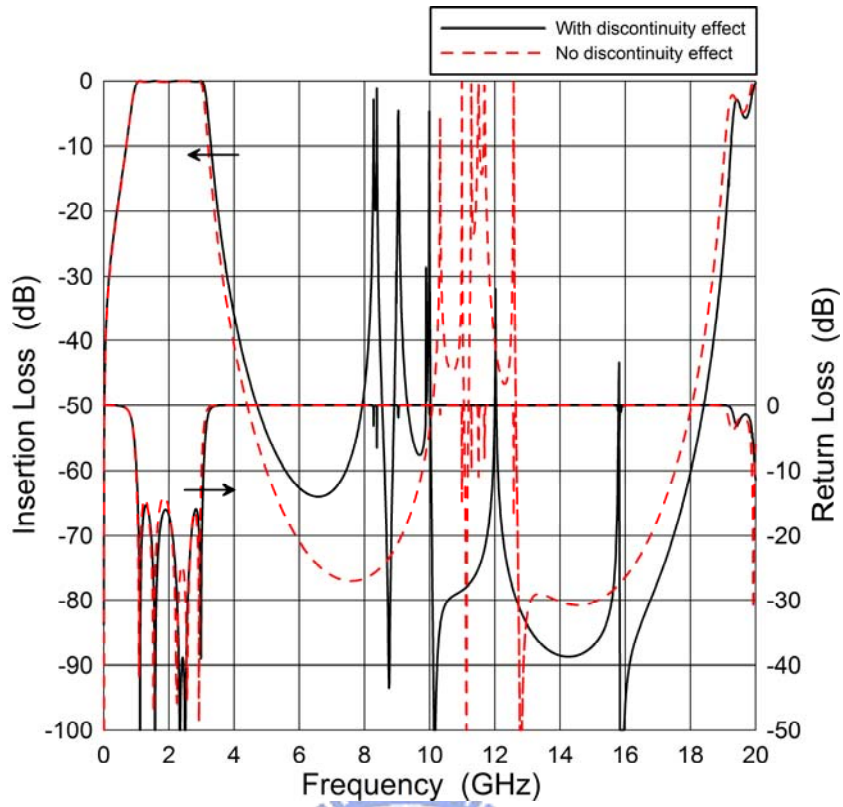
Fig. 4-17. Simulated results of the proposed stepped-impedance wideband bandpass filter by using the circuit simulator.

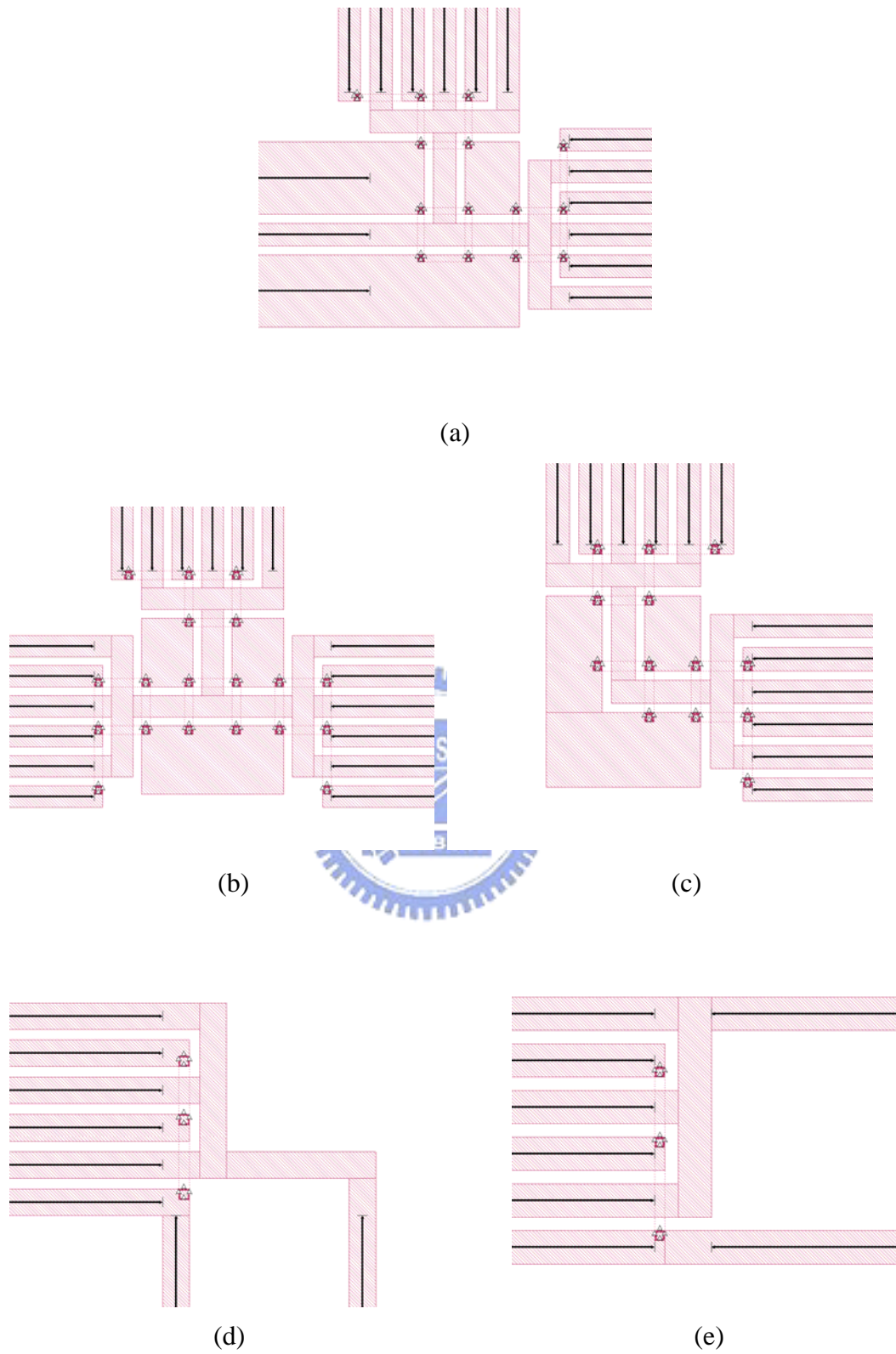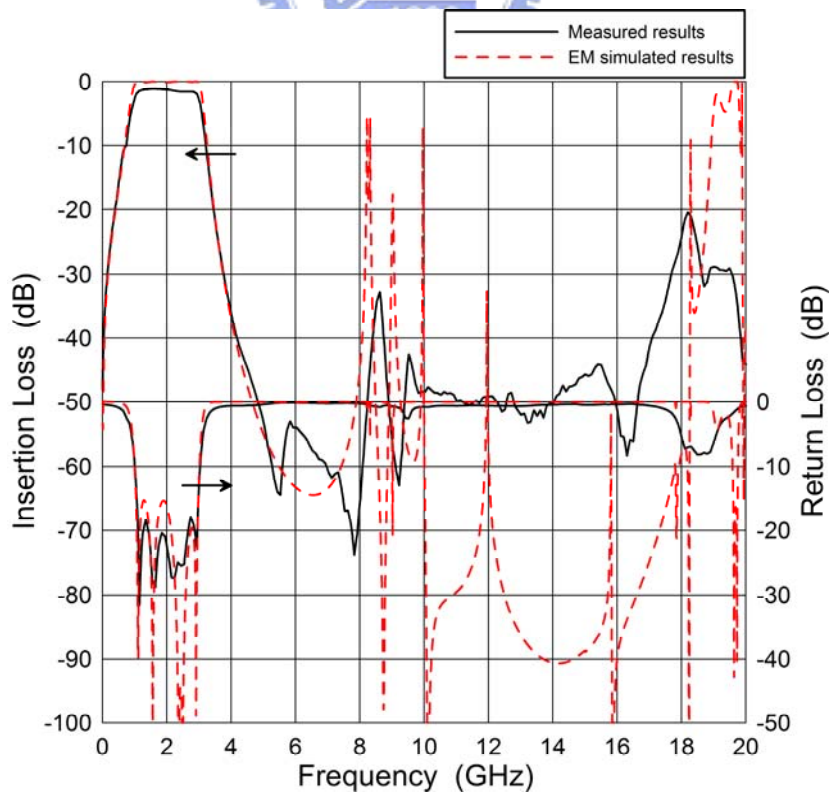Fig. 4-18. EM simulated results and measured results of the proposed bandpass filter.
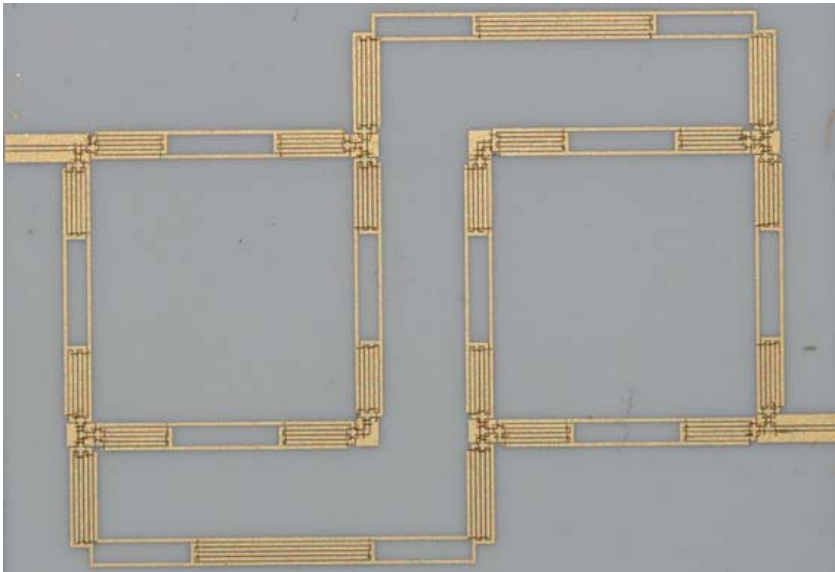
Fig. 4-19. Photograph of the fabricated stepped-impedance wideband bandpass filter.

Chapter 5

Conclusion

In this dissertation, several novel 180^0 hybrid couplers have been proposed and implemented with microstrip and uniplanar structure. Then, on the basis of these 180^0 hybrid couplers, a new class of wideband bandpass filters is presented.

The 180^0 hybrid ring coupler using a novel interdigital CPS phase inverter has been designed and fabricated to exhibit size reduction and wideband performance. Extremely low/high impedances can be obtained by using CPS/interdigital CPS. With design equations for the stepped-impedance and design curves for CPS/interdigital CPS, the proposed hybrid ring coupler can be readily designed. This hybrid provides good amplitude and phase characteristic and good isolation over a wide bandwidth due to the phase inverter being independent of frequency. This circuit shows about 87% size reduction compared to the conventional $3/2\lambda$ CPS hybrid ring.

Based on the reconfigured the ideal single-section hybrid ring, the wideband two-section hybrid rings with Chebyshev characteristics have been developed for bandwidth enhancement, size reduction, and high power-division ratios. In addition, the two-section hybrid ring by cascading of two single-section unit with a unit element at each I/O port is presented for further bandwidth improvement. The short-ended VIP coupler has been successfully used to approach an ideal

single-section unit. It also provides a good crossover for realization of the circuit. Thus, the wideband multi-section hybrid rings using the VIP coupler are suitable for microstrip implementation.

By cascading two 180^0 hybrid rings with one or two pairs of 90^0 transmission lines, a stepped-impedance wideband bandpass filter has been designed and fabricated to exhibit wide passband and broad stopband performance simultaneously. In addition, the bandwidth can be further enhanced by cascading more sections of 90^0 transmission lines between two rat-race hybrid couplers or at each I/O port of the rat-race hybrid coupler in the proposed structure. All the measured results show good agreements with the simulated responses. With provided design equations, design curves and design procedures for all above-mentioned circuit, these circuits can be designed systematically.

In the future work, the performance of the proposed wideband bandpass filter can be improved with transmission zeros for the both upper and lower cutoff selectivity enhancement.

Reference

[1] T. Hirota, A. Minakawa, and M. Muraguchi, "Reduced-size branch-line and rat-race hybrids for uniplanar MMIC's," *IEEE Trans. Microw. Theory Tech.*, vol. 38, pp. 270–275, Mar. 1990.

[2] H.-R. Ahn, I. S. Chang, and S.-W. Yun, "Miniaturized 3-dB ring hybrid terminated by arbitrary impedances," *IEEE Trans. Microw. Theory Tech.*, vol. 42, no. 12, pp. 2216–2221, Dec. 1994.

[3] D. I. Kim and G.-S. Yang, "Design of new hybrid-ring directional coupler using λ/8 or λ/6 sections," *IEEE Trans. Microw. Theory Tech.*, vol. 39, no. 10, pp. 1779–1784, Oct. 1991.

[4] R. K. Settaluri, G. Sundberg, A.Weisshaar, and V. K. Tripathi, "Compact folded line rat-race hybrid couplers," *IEEE Microw. Guided Wave Lett.*, vol. 10, no. 2, pp. 61–63, Feb. 2000.

[5] K. W. Eccleston and S. H. M. Ong, "Compact planar microstripline branch-line and rat-race coupler," *IEEE Trans. Microw. Theory Tech.*, vol. 51, no. 10, pp. 2119–2125, Oct. 2003.

[6] S. March, "A wideband stripline hybrid ring," *IEEE Trans. Microw. Theory Tech.*, vol. MTT-16, p.361, June 1968.

[7] M. K. Mandal and S. Sanyal, "Reduced-Length Rat-Race Couplers," *IEEE Trans. Microwave Theory Tech.*, vol.55, no.12, pp. 2593-2598, part1, Dec. 2007.

[8] H. Okabe, C. Caloz, and T. Itoh, "A compact enhanced-bandwidth hybrid ring using an artificial lumped-element left-handed transmission-line section," *IEEE Trans. Microw. Theory Tech.*, vol. 52, no. 3, pp. 798–803, Mar. 2004.

[9] C. -Y. Chang and M. -F Hsieh, "Miniaturized broadband rat-race ring coupler," in *2003 APMC Dig.*, Seoul, Korea, pp. 1700-1703, Nov. 2003.

[10] C.-H. Ho, L. Fan, and K. Chang, "New uniplanar coplanar waveguide hybrid-ring couplers and magic-T's," *IEEE Trans. Microw. Theory Tech.*, vol. 42, no. 12, pp. 2440–2448, Dec. 1994.

[11] L. Fan, C. H. Ho, and K. Chang, "Wide-band reduced-size uniplanar magic-T, hybrid-ring, and de Ronde's CPW-slot couplers," *IEEE Trans. Microw. Theory Tech.*, vol. 43, pp. 2749–2758, Dec. 1995.

[12] B. R. Heimer, L. Fan, and K. Chang, "Uniplanar hybrid couplers using asymmetrical coplanar striplines," *IEEE Trans. Microw. Theory Tech.*, vol. 45, no. 12, pp. 2234–2240, Dec. 1997.

[13] T. Wang and K. Wu, "Size-reduction and band-broadening design technique of uniplanar hybrid ring coupler using phase inverter for M(H)MIC's," *IEEE Trans. Microw. Theory Tech.*, vol. 47, no. 2, pp.198–206, Feb. 1999.

[14] C.-W. Kao and C. H. Chen, "Novel uniplanar 180 hybrid-ring couplers with spiral-type phase inverters," *IEEE Microw. Guided Wave Lett.*, vol. 10, no. 10, pp. 412–414, Oct. 2000.

[15] T. T. Mo, Q. Xue and C. H. Chan, "A Broadband Compact Microstrip Rat-Race Hybrid Using a Novel CPW Inverter," *IEEE Trans. Microwave Theory Tech.*, vol. 55, no. 1, pp. 161-167, Jan. 2007.

[16] L. K. Yeung and Y. E. Wang, " A Novel 180° Hybrid Using Broadside-Coupled Asymmetric Coplanar Striplines," *IEEE Trans. Microwave Theory Tech.*, vol.55, no.12, pp. 2625-2630, part1, Dec. 2007.

[17] S. Rehnmark, "Wide-band balanced line microwave hybrids," *IEEE Trans. Microw. Theory Tech.*, vol. MTT-25, pp. 825-830, Oct. 1977.

[18] C. Y. Chang and C. C. Yang, "A novel broad-band Chebyshev-response rat-race ring coupler, " *IEEE Trans. Microwave Theory Tech.*, vol. 47, pp.455-462, Apr. 1999.

[19] A. K. Agrawal and G. F. Mikucki, "A printed circuit hybrid-ring directional coupler for arbitrary power divisions," *IEEE Trans. Microwave Theory Tech.*, vol. MTT-34, pp. 1401-1407, Dec. 1986.

[20] R. Levy and L. F. Lind, "Synthesis of symmetrical branch-guide directional couplers," *IEEE Trans. Microwave Theory Tech.*, vol. MTT-16, pp. 80-89, Feb. 1968.

[21] K. S. Ang, Y. C. Leong, and C. H. Lee, "A new class of multisection 180° hybrids based on cascadable hybrid-ring couplers" *IEEE Trans. Microwave Theory Tech.*, vol. 50,   pp. 2147-2152, Sep.2002.

[22] G. L. Matthaei, "Design of wide-band (and narrow-band) band-pass microwave filters on the insertion loss basis," *IEEE Trans. Microwave Theory Tech., vol. 8, no.6*, pp. 580-593, Nov. 1960.

[23] J.-T. Kuo and E. Shih, "Wideband bandpass filter design with three-line microstrip structures," *IEE Proceedings on Microwaves, Antennas and Propagation*, vol. 149, pp. 243-247, Oct.-Nov. 2002.

[24] L. Zhu, H. Bu, and K. Wu, "Aperture compensation technique for innovative design of ultra-broadband microstrip bandpass filter," in *IEEE MTT-S Int. Microw. Symp. Dig.*, Boston, MA, Jun. 2000, vol. 1, pp.315–318.

[25] C.-H. Chi, and C.-Y. Chang, "Wideband Chebyshev-response bandpass filter by cascading of cascadable 180° hybrid rings," in *APMC 2006 Dig.,* Yokohama, Japan, pp. 151-154, Dec. 2006.

[26] L. Zhu, S. Sun and W. Menzel, "Ultra-wideband (UWB) bandpass filters using multiple-mode resonator," *IEEE Microwave Wireless Components Letters*., vol. 15, no. 11, pp. 796-798, Nov. 2005.

[27] J. Gao, L. Zhu, W. Menzel and F. Bogelsack, "Short-circuited CPW multiple-mode resonator for ultra-wideband (UWB) bandpass filter." *IEEE Microwave Wireless Components Letters.*, vol. 16, no. 3, pp. 104-106, Mar. 2006.

[28] Y.-C. Chiou, J.-T. Kuo, and E. Cheng, "Broadband quasi-Chebyshev bandpass filters with multimode stepped-impedance resonators (SIRs)." *IEEE Trans. Microwave Theory Tech.*, vol. 54, no. 8, pp. 3352-3358, Aug. 2006.

[29] R. Li and L. Zhu, "Compact UWB bandpass filter using stub-loaded multiple-mode resonator," *IEEE Microw. Wireless Compon. Lett.*, vol.17, no. 1, pp. 40–42, Jan. 2007.

[30] S. W. Wong and L. Zhu "EBG-Embedded Multiple-Mode Resonator for UWB Bandpass Filter With Improved Upper-Stopband Performance," *IEEE Microw. Wireless Compon. Lett.*, vol.17, no. 6, pp. 421–423, Jane 2007.

[31] S. Sun and L. Zhu*,* "Wideband Microstrip Ring Resonator BandpassFilters Under Multiple Resonances," *IEEE Trans. Microwave Theory Tech.*, vol. 55, no. 10, pp. 2176-2182, Oct. 2007.

[32] L.-H. Hsieh and K. Chang, "Compact, low insertion-loss, sharp-rejection, and wide-band microstrip bandpass filters," *IEEE Trans. Microwave Theory Tech.*, vol. 51, no. 4, pp. 1241-1246, Part 1, April 2003.

[33] H. Ishida and K. Araki, "Design and analysis of UWB bandpass filter with ring filter" *2004 IEEE MTT-S Int. Microwave Symp. Dig.*, vol. 3, pp.1307-1310, June 2004.

[34] C.-L. Hsu, F.-C. Hsu, and J.-T. Kuo, "Microstrip bandpass filters for ultra-wideband (UWB) wireless communications," in *IEEE MTT-S Int. Dig.*, Jun. 2005, pp. 679–682.

[35] M. Makimoto and S. Yamashita, "Bandpass filters using parallel coupled stripline stepped impedance resonators," *IEEE Trans. Microwave Theory Tech.*, vol. 28, no. 12, pp. 1413-1417, Dec. 1980.

[36] Y. Konishi, I. Awai, Y. Fukuoka, and M. Nakajima." A directional coupler of a vertically installed planar circuit structure" *IEEE Trans. Microwave Theory Tech.* vol. 36, pp. 1057-1063, June 1988.

[37] J. A. Dobrowolski, Introduction to Computer Methods for Microwave Circuit Analysis and Design. Norwood, MA: Artech House, 1991, pp.81-90.

[38] H. J. Riblet, "The application of a new class of equal-ripple functions to some familiar transmission-line problems," *IEEE Trans. Microwave Theory Tech.*, vol. MTT-12, pp. 415-421, July 1964.

[39] H. J. Carlin and W. Kohler, "Direct synthesis of band-pass transmission line structures," *IEEE Trans. Microwave Theory Tech.*, vol. MTT-13, pp. 283-297, May 1965.

[40] HFSS, ver. 9.2, Ansoft, Pittsburgh PA, 2004.